Progress in Nuclear Magnetic Resonance Spectroscopy 54 (2009) 166–182

Contents lists available at ScienceDirect

Progress in Nuclear Magnetic Resonance Spectroscopy

journal homepage: www.elsevier.com/locate/pnmrs

NMR in the Earth's magnetic field

Aleš Mohorič [a], Janez Stepišnik [a,b,*]

[a] Faculty of Mathematics and Physics, University of Ljubljana, Jadranska 19, 1000 Ljubljana, Slovenia
[b] "Jožef Stefan" Institute, Jamova 39, 1000 Ljubljana, Slovenia

ARTICLE INFO

Article history:
Received 26 May 2008
Accepted 16 July 2008
Available online 3 August 2008

Contents

1. Introduction

The development of NMR methods in high magnetic fields has opened the door to many applications in the last decades. A trend to higher magnetic fields produced by large and expensive superconducting magnets took place because the signal-to-noise ratio (S/N) and the dispersion of different NMR lines improve with increasing field strength. Parallel to the development of NMR in strong magnetic fields, the potential of NMR in low-magnetic fields (<mT) is being explored. Since 1954, Earth's field NMR (EFNMR) [1] has been something of a curiosity, used primarily for geophysical magnetometry, or as a simple low-cost demonstration of magnetic resonance principles, but has continued to attract attention [2–6] because some information accessible in low fields is hard to obtain in high fields. For instance, it has been shown with various rat tissues [7] that the $1/T_1$ dependence on magnetic field strength has an inflection below 0.01 T and other reports also show the benefits of low-field relaxation measurements [8,9].

In the early days of magnetic resonance imaging (MRI) the price of superconducting magnets led to considerations of ultralow MRI

* Corresponding author. Address: Faculty of Mathematics and Physics, University of Ljubljana, Jadranska 19, 1000 Ljubljana, Slovenia.
E-mail address: Janez.Stepisnik@fmf.uni-lj.si (J. Stepišnik).

0079-6565/$ - see front matter
doi:10.1016/j.pnmrs.2008.07.002

[10] and as early as 1984 first reports on Earth's field MRI appeared [11–16]. These first experiments used the method of Packard and Varian [1] of pre-magnetization, with the rapid switch-off and back projection method [17], and usually employed aluminum boxes for shielding of electromagnetic noise. In 1982 it was shown that EFNMR was amenable to the same oscillating magnetic field pulse techniques as its high-field counterpart [18]. Later imaging systems evolved [19,20] to incorporate a full 3D gradient set [21] and enable magnetization manipulation with audio frequency (AF) oscillating magnetic pulses. Mobility is another important factor since EFNMR apparatus requires no magnet, and because everything on Earth is immersed in its field, and potentially subject to its influence. The portability of the apparatus led to some unique research on diffusion in Antarctic ice [22–26] and ground water explorations [27,28].

As the strength of the measurement field is reduced, it is possible to achieve very narrow NMR lines and the associated high *S*/*N* and spectral resolution. At such low fields scalar couplings, which are field-independent, are preserved. As early as 1965, Béné et al. showed that it is possible to measure heteronuclear *J*-couplings in EFNMR [29]. Since high homogeneity and stability of the low field can be successfully achieved, experiments have confirmed that many important spin multiplets can be studied at low fields. Recently, it was shown that chemical shift differences can be measured even in inhomogeneous low-magnetic fields [30,31]. In the Earth's magnetic field the chemical shift of hyper-polarized xenon ^{129}Xe has been measured with a precision similar to that obtainable at high fields [32]. Proton ^{1}H and fluorine ^{19}F EFNMR spectra were acquired with a frequency resolution nearly two orders of magnitude better than obtainable by high-resolution NMR in high field [33]. It was recently shown that it is possible to observe heteronuclear *J*-couplings via the classic COSY experiment [34]. The first observation of homonuclear proton *J*-couplings in the Earth's magnetic field, which earlier seemed to be impossible [35,36], was recently reported [37]. In condensed-matter physics, where in high fields dipole–dipole interactions lead to substantial line broadening, the use of low fields in solids allows spectra with a high resolution to be obtained [38]. So-called "forbidden transitions" are another example of information observable only in low-magnetic fields [39].

An obvious draw-back of low-field experiments is the weak equilibrium polarization of nuclear spins, which scales with the magnetic field. The loss in polarization can be circumvented by one of several techniques which create enhanced, non-equilibrium nuclear spin polarization, such as dynamic nuclear polarization (DNP) [40–42], optical pumping [43], or pre-magnetization [1]. For large samples, the sensitivity of the experiment can also be improved by increasing the number of turns of the detecting coil. However, as long as Faraday coil detection is used, the signal amplitude still scales with magnetic field and the sensitivity can be boosted by detecting the signal with a superconducting quantum interference device (SQUID) [44], which is sensitive to magnetic flux, rather than the rate of change of flux. When operated with an untuned (superconducting) input circuit, SQUID detects broadband at arbitrarily low frequencies without a loss in sensitivity. SQUIDs have been used successfully since the 1980s to detect NMR signals [45]. The majority of SQUID NMR measurements have been performed on samples in the solid state at liquid helium temperatures. However, more recently, samples at room temperature were imaged in fields of several millitesla using SQUIDs [46] and spectra from animal tissue at room temperature were measured [47]. A SQUID magnetometer fabricated from a high-transition temperature superconductor was used to image thermally polarized proton samples at room temperature in low field [48]. In later experiments, SQUID was used to measure NMR signals from samples in microtesla fields [49]. With pre-magnetization in 100–500 mT fields, one can acquire two-dimensional proton MR images of water and oil phantoms, a cross-sectional view of fruits, three-dimensional (3D) images of phantoms [50] and in vivo images of a human forearm and fingers [51].

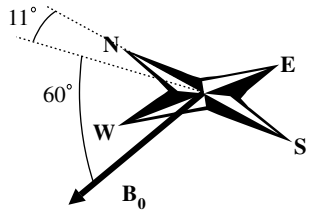

Fig. 1. The Earth's magnetic field at the site of the Ljubljana EFNMR system.

Other applications of EFNMR are detection of free induction decay [52,18,53–55] and diffusion measurements [34,50]. Experiments carried out on the Ljubljana EFNMR system such as diffusion measurements [56], MRI [21], flow measurements and flow distribution [57], measurements of diffusion distributions [58], and natural convection studies [59] are described in more detail in Section 9.

2. The Earth's magnetic field

EFNMR is measured in the Earth's magnetic field which is approximately a dipole field, and in Europe has a declination of 11° and an inclination of 30° as shown in Fig. 1. In the zone of Europe and North America its magnitude is close to 50 μT. The Larmor frequency for protons is thus around 2 kHz and lies in the AF range. By proper shielding against electromagnetic noise, short time variation of 10^{-11} T/s and a spatial gradient smaller than 10^{-10} T/m can be achieved. Measurements show a gradient of 10^{-12} T/m and non-correlated variations of 2.5×10^{-8} T/year, 5×10^{-8} T during the day and oscillations of 10^{-9} T with a period of about 25 s, caused by variations in the ionospheric current and as a result of intraterrestial causes [2,60].

3. Temporal evolution of spins

Spins evolve in a uniform, static magnetic field B_0. In further discussion the *z*-axis of our coordinate system is aligned along B_0. Certain NMR techniques for imaging and migration measurements require an oscillating magnetic field (radiofrequency (RF) in high field and AF in low field) and a non-uniform magnetic field, commonly in the form of pulses. The temporal evolution of magnetization in changing magnetic fields is quite commonly treated by modified Bloch equations [41] using numerical and iterative approaches [61,62]. Herein, we show that the temporal evolution of spins in a variable magnetic field can be solved elegantly using the Hamiltonian approach. The general Hamiltonian of a spin system in a magnetic field $\boldsymbol{B}$ is

$$H(t) = -\sum_j \boldsymbol{\mu}_j \cdot \boldsymbol{B}(t, \boldsymbol{r}_j) = -\gamma\hbar \sum_j \boldsymbol{I}_j \cdot \boldsymbol{B}(t, \boldsymbol{r}_j) \tag{1}$$

where the *j*th spin with its magnetic moment interacts with the magnetic field at its location $\boldsymbol{r}_j$.

Usually in EFNMR the spins are initially magnetized by a strong magnetic field applied perpendicular to the Earth's magnetic field (in our case along the *x*-axis) as shown in Fig. 2. This field need not be fully uniform, but its magnitude is reduced for the period of spin manipulation and signal detection.

The factorized Hamiltonian

$$H(t) = H_{\mathrm{m}}(t) + H_0 + H_{\mathrm{rf}}(t) + H_{\mathrm{g}}(t) + H_{\mathrm{ss}} + H_{\mathrm{L}} \tag{2}$$

consists of terms of the form of Eq. (1) describing the interaction of spins with the pre-magnetizing field $\boldsymbol{B}_{\mathrm{m}}(t)$, the uniform Earth's magnetic field $\boldsymbol{B}_0$, the oscillating magnetic field $\boldsymbol{B}_{\mathrm{rf}}(t)$ applied per-

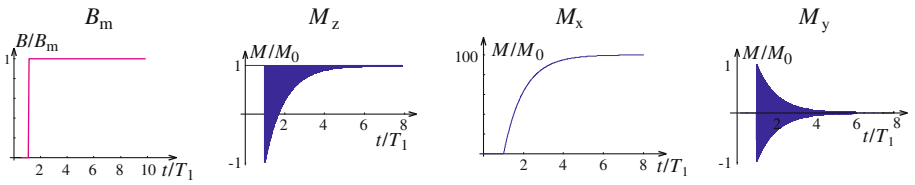

Fig. 2. The evolution of all three components of magnetization in the field B_0 along the z-axis and the pre-magnetizing field along the x-axis. The magnitude of the pre-magnetizing field is $B_m = 100B_0$ and the field is switched on instantly. The magnetization relaxes to its new equilibrium value M_0 with a characteristic time T_1. In this numerical solution of the Bloch equations, the approximation $T_1 = T_2$ is used. The blue fill in M_z and M_y is the consequence of rapid oscillations.

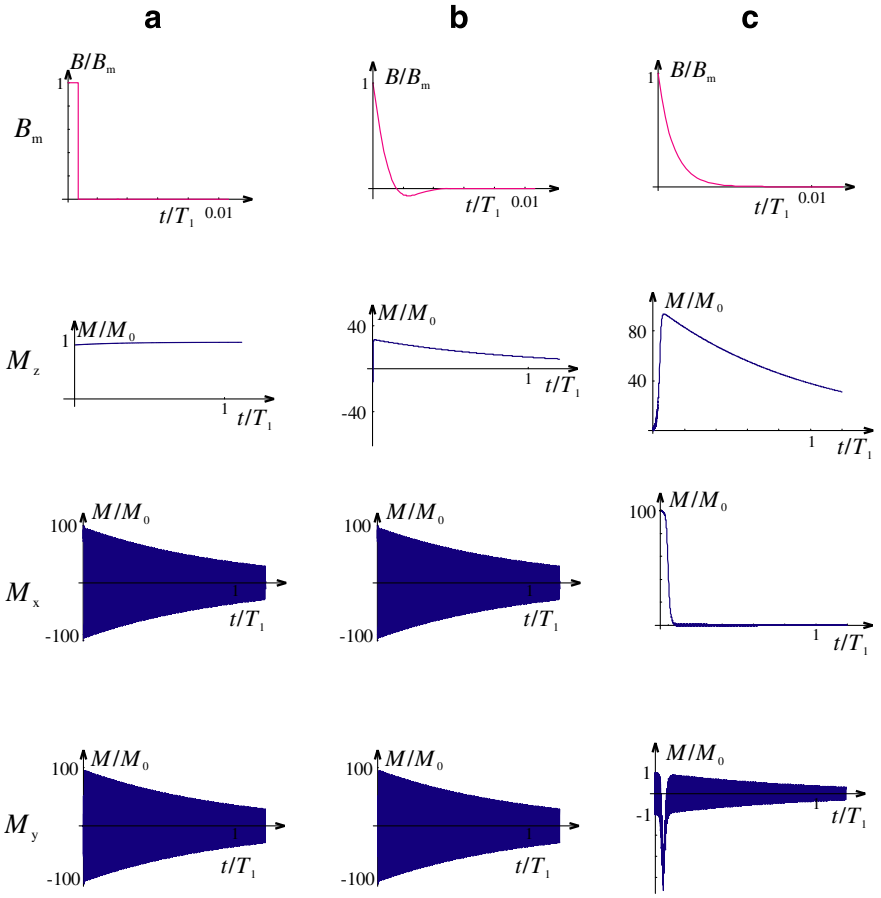

Fig. 3. Evolution of magnetization after cut-off of the pre-magnetizing field B_m aligned along the x-axis with magnitude $100B_0$, B_0 points along the z-axis. Three different cases are shown: (a) instant, (b) damped sine, and (c) exponential cut-off. Only the exponential cut-off produces a negligiable transverse relaxation. In this numerical solution of the Bloch equations, the approximation $T_1 = T_2$ is used. Blue fills in M_x and M_y plots are the consequence of rapid oscillations.

pendicular to the Earth's field and, in the case of MRI or diffusion measurements, also with the non-uniform magnetic field $\boldsymbol{B}_g(t, \boldsymbol{r}_j)$ that encodes spin location or motion. Remaining interactions include spin–spin interactions and spin interactions with internal fields H_{ss}, as well as the spin–molecular or the spin–lattice interaction included in H_L.

Following the usual practice, we use the density matrix approach [63] with

$$\rho(t) = U(t)\rho(0)U^{-1}(t) \tag{3}$$

to describe the state of the system, which evolves from the initial state $\rho(0)$ according to the time evolution operator

$$U(t) = \widehat{T}\mathrm{e}^{-\mathrm{i}/\hbar \int_0^t H(t')\,\mathrm{d}t'} \tag{4}$$

where $\widehat{T}$ is the time ordering operator which imposes a successive order of time-dependent interactions. The timing scheme of the magnetic resonance experiment in the Earth's magnetic field can most commonly be separated into three distinctive stages: the pre-magnetization period, the switching period and the excitation–manipulation–evolution–detection period. This helps in the evaluation of the time evolution operator, since the end state of the preceding step is the initial state of the following step.

3.1. Pre-magnetization

Usually in low-field NMR the technique of Varian and Packard is used [1,2] where a pre-magnetizing field perpendicular to the Earth's magnetic field is applied to the sample at the beginning of each experiment (Fig. 2). When the magnetization reaches its new equilibrium value, this field is switched off. The alignment of the resulting magnetization depends on the rate and the manner of pre-magnetizing field switching. As shown in Fig. 3 and in the following derivation, the magnetization retains its direction transverse to B_0 for a very fast switching rate, i.e., when the field cut-off is shorter than the Larmor period, or when the field decays in an oscillatory manner with the frequency of the precession in the low-magnetic field. Whenever the pre-magnetizing field is switched-off with a rate slow compared to the spin precession period, the magnetization fol-

lows the effective field. The vector sum of $\boldsymbol{B}_m$ and $\boldsymbol{B}_0$ ends up aligned along B_0. We will count the time in expressions (3) and (4) from the moment when the pre-magnetization is completed and the switching period starts. Thus, the initial spin density matrix in the high-temperature approximation is determined by the magnetization produced by the pre-magnetizing field as

$$\rho(0) = \rho_L\left(1 - \beta\hbar\gamma\sum_j B_m(\boldsymbol{r}_j)I_{jx}\right) \tag{5}$$

where $\beta = 1/k_BT$ and the product $\beta\hbar\gamma B_m(\boldsymbol{r}_j)$ describes the degree of magnetization at the location of the jth spin if the pre-magnetizing field is not uniform; ρ_L is the lattice density matrix operator. Assuming the prevailing effect of the pre-magnetizing field during the switching period $(0, t_s)$ and neglecting the effect of H_L, the spin evolution is described by

$$U(t_s) = \widehat{T}e^{-i/\hbar\int_0^{t_s}[H_0+H_m(t')]dt'} \tag{6}$$

By neglecting the interactions between spins we can write

$$U(t_s) = \prod_j U_j(t_s) \tag{7}$$

with

$$U_j(t_s) = \widehat{T}e^{-i\gamma\int_0^{t_s}[I_{jx}B_m(t',\boldsymbol{r}_j)+I_{jz}B_0]dt'} \tag{8}$$

The time ordering in Eq. (6) prevents a straightforward integration of the exponent and an approximation for the time evolution operator that depends on the manner of field switching is needed.

3.1.1. Adiabatic magnetic field switching

The rotation of initial magnetization from the direction of the pre-magnetizing field, to the direction of Earth's field can be achieved by a slow (adiabatic) decay of B_m as

$$B_m(t) = B_{m0}e^{-t/t_m} \tag{9}$$

As B_m points along the x-axis and B_0 along the z-axis, the spin coordinate system is transformed by the rotation operator

$$R_j(t) = e^{-i\int_0^t\dot{\varphi}_j(t')I_{jy}dt'} \tag{10}$$

with

$$\varphi_j(t) = \arctan\frac{B_m(t,\boldsymbol{r}_j)}{B_0} \tag{11}$$

and

$$\dot{\varphi}_j(t) = \frac{d\varphi_j(t)}{dt} \tag{12}$$

into a local frame with its z-axis pointing along the effective magnetic field

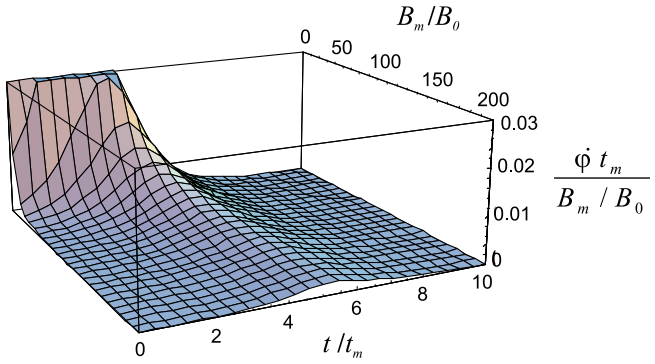

Fig. 4. Time evolution of $\dot{\varphi}(t)$ perturbation of the effective magnetic field for exponential decay of the pre-magnetizing field at various magnitudes B_m/B_0.

$$B_{tot}(t,\boldsymbol{r}_j) = \sqrt{B_m^2(t,\boldsymbol{r}_j) + B_0^2} \tag{13}$$

The factoring theorem [64] permits the factorization of the single spin operator in Eq. (6) into

$$U_j(t) = R_j(t)\times\widehat{T}e^{i\int_0^{t_s}[\dot{\varphi}_j(t)I_{jy}+\gamma B_{tot}(t,\boldsymbol{r}_j)I_{jz}]dt} \tag{14}$$

In the case of exponential decay of the pre-magnetizing field, the time derivative of the rotation angle $\dot{\varphi}(t) = -\frac{\frac{B_{m0}}{t_m B_0}e^{-t/t_m}}{\left(\frac{B_{m0}}{B_0}e^{-t/t_m}\right)^2+1}$ with the maximum $\dot{\varphi}_{max} = -\frac{1}{2}\frac{1}{t_m}$ at $t = t_m\ln\frac{B_{m0}}{B_0}$ is as shown in Fig. 4. If the condition $1/t_m \ll \gamma B_{m0}$ is satisfied, the first term in Eq. (14) can be neglected.

During the decay of the pre-magnetizing field $\varphi(t)$ changes by almost $\pi/2$ if $B_m \gg B_z$. In this case the magnetization, the magnetic dipole moment per unit volume, after uniform pre-magnetization of N identical spins occupying volume V can be calculated as

$$M = \hbar\gamma\sum_j TrU_j(t)\rho(0)U_j^*(t)I_{jz}/V = -\beta\hbar^2\gamma^2I(I+1)B_m n/3 \tag{15}$$

where $n = N/V$ is the number density of spins and

$$U(t) = \prod_j e^{-i\frac{\pi}{2}I_{jy}}e^{i\int_0^{t_s}\gamma B_{tot}(t,\boldsymbol{r}_j)I_{jz}dt} \tag{16}$$

Slow decay of the magnetic field compared to the spin precession period in the strong field turns the spin magnetization into the direction of the Earth's magnetic field. For instance, pre-magnetization in a field of 0.05 T requires a decay of about a few milliseconds to fulfill the adiabatic condition. In the case of a reversible process, where the magnetization is slowly increased, the magnetization will again follow the direction of effective magnetic field.

3.2. Oscillatory decay of the pre-magnetizing field

Magnetization can be preserved in the plane perpendicular to B_0 if the pre-magnetizing field is switched-off within a few attenuated oscillations

$$B_m(t) = B_{m0}e^{-t/t_m}\cos\omega t \tag{17}$$

where ω is close to the Larmor frequency of the terminal geomagnetic field, $\omega_0 = \gamma B_0$. Using the factoring theorem, the time evolution operator can be written

$$U(t) = \widehat{T}e^{-i/\hbar\int_0^{t_s}[H_0+H_m(t')]dt'} = e^{-iH_0t/\hbar}\times\widehat{T}e^{-i/\hbar\int_0^{t_s}\widetilde{H}_m(t')dt'} \tag{18}$$

where

$$\begin{aligned}\widetilde{H}_m(t) &= e^{iH_0t/\hbar}H_m(t')e^{-iH_0t/\hbar}\\ &= \hbar\gamma\sum_j B_{m0}(I_{jx}\cos\omega_0t - I_{jy}\sin\omega_0t)e^{-t/t_m}\cos\omega t\end{aligned} \tag{19}$$

With the second order Magnus expansion (Appendix I) it is easy to show that for $t_s \gg t_m$ with $\omega \approx \omega_0$ we can approximate

$$\widehat{T}e^{-i/\hbar\int_0^{t_s}\widetilde{H}_m(t')dt'} \approx \prod_j e^{i\gamma B_{m0}t_m\left(\frac{1}{2}I_{jx}-\frac{\omega_0t_m}{1+4(\omega_0t_m)^2}I_{jy}\right)+\cdots} \tag{20}$$

The second and all higher exponential terms are small compared to the first one if $\omega_0t_m > 1$. For instance, when $\omega_0t_m = 5$ its partition in the Hamiltonian is about 5%, allowing the approximation

$$U_j(t) = e^{i\omega_0I_{jz}t}e^{i\gamma B_{m0}I_{jx}t_m/2} \tag{21}$$

Acting on the initial spin state Eq. (5), this evolution operator gives the precession of the initial magnetization in the xy-plane perpendicular to the direction of the Earth's magnetic field. This effect

can be understood as a magnetization locking in the transverse direction to B_0. This method can be employed on the special system working in the Earth's magnetic field, where an auxiliary NMR (which we call the reference NMR coils) controls the spin excitation and detection in the main NMR. In this way, the NMR set-up can work coherently with the clock set by Larmor precession in the instantaneous magnetic field.

The high inductance of the pre-magnetizing coils prevents switching with a rate faster than the spin precession period, so oscillatory switching-off that preserves the spin precession in the *xy*-plane without applying a $\pi/2$ pulse is used instead.

4. Spin position encoding by a non-uniform magnetic field

Combination of the static uniform field B_0 and non-uniform magnetic field is used to determine the spatial distribution of nuclear spins (magnetic resonance imaging) and their migration either as flow or diffusion. In a measurement of diffusion with EFNMR [56] the necessary spin dephasing is brought about by a non-uniform magnetic field that is comparable to or larger than B_0. In this case the non-uniform component of the field is of the same order of magnitude as the uniform one. Large non-uniform fields imply deviations from a simple linear relation between the intensity of the magnetic field and one space coordinate (the direction of the field gradient in the conventional magnetic field gradient representation). Here, we show how the signal should be analyzed under the influence of such a strong non-uniform field. Neglecting all other interactions but the effect of the uniform magnetic field along the *z*-axis and of the non-uniform magnetic field with its orientation depending on the location of spin, the Hamiltonian is

$$H = H_g + H_0 \tag{22}$$

with

$$H_g = -\hbar\gamma \sum_j \boldsymbol{B}_g(\boldsymbol{r}_j, t)\cdot \boldsymbol{I}_j \tag{23}$$

If the positional correlation between different spins is neglected, the time evolution operator can again be factorized in the manner shown for the adiabatic switching of the pre-magnetizing field giving

$$U_j(t) = \widehat{T}\mathrm{e}^{\mathrm{i}\int_0^t [\omega_0 I_{jz} + \gamma \boldsymbol{B}_g(t', \boldsymbol{r}_j)\cdot \boldsymbol{I}_j]\mathrm{d}t'} \tag{24}$$

The time evolution operator transformed into the frame with the *z*-axis oriented along the total magnetic field at the site of the particular spin, $\boldsymbol{B}_{\mathrm{tot}} = \boldsymbol{B}_0 + \boldsymbol{B}_g(t, \boldsymbol{r}_j)$ can be written

$$U_j = \widehat{T}\mathrm{e}^{\mathrm{i}\int_0^t [\dot{\boldsymbol{\varphi}}(\boldsymbol{r}_j, t')\cdot \boldsymbol{I}_j + \omega_{\mathrm{tot}}(\boldsymbol{r}_j, t') I_{jz}]\,\mathrm{d}t'} R_j(t) \tag{25}$$

where $\omega_{\mathrm{tot}} = \gamma \mid \boldsymbol{B}_{\mathrm{tot}} \mid$ and

$$R_j(t) = \mathrm{e}^{-\mathrm{i}\sum_j \int_0^t \dot{\boldsymbol{\varphi}}(\boldsymbol{r}_j, t')\cdot \boldsymbol{I}_j \mathrm{d}t'} \tag{26}$$

which represents rotation around the axis perpendicular to the plane formed by the *z*-axis and $\boldsymbol{B}_{\mathrm{tot}}$ (see the Appendix). In the case of slow field variation, i.e., adiabatic switching of a non-uniform field

$$|\dot{\boldsymbol{\varphi}}[\boldsymbol{r}_j(t), t]| \ll \omega_{\mathrm{tot}}[\boldsymbol{r}_j(t), t] \tag{27}$$

one can neglect the angular velocity $|\dot{\boldsymbol{\varphi}}[\boldsymbol{r}_j(t), t]|$ in Eq. (25) with respect to the effective precession frequency of the *j*th spin. In nearly all experiments the non-uniform magnetic field returns to zero and consequently the net rotation at the end of the non-uniform magnetic field pulses is simply $R_j(t) \equiv 1$. (The only practical case where this return of applied fields to zero may not apply concerns the use of read gradients in imaging.) We are therefore able to reduce Eq. (25) into a simpler expression, giving

$$U_j(t) = \mathrm{e}^{\mathrm{i}\sum_j \int_0^t \omega_{\mathrm{tot}}(\boldsymbol{r}_j, t') I_{jz}\,\mathrm{d}t'} \tag{28}$$

with only the *z*-component of the spin operator. The evolution operator now represents the rotation around a (locally defined) *z*-axis.

In the particular case when the main field is much stronger than the non-uniform field $\omega_0 \gg \gamma \mid \boldsymbol{B}_g(\boldsymbol{r}) \mid$, the effective spin precession can be simplified as

$$\begin{aligned}\omega_{\mathrm{tot}}(\boldsymbol{r}_j + \Delta\boldsymbol{r}_j) &= \omega_0 + \gamma\nabla|\boldsymbol{B}_g(\boldsymbol{r}_j)|\cdot\Delta\boldsymbol{r}_j + \cdots \\ &\approx \omega_0 + \gamma \boldsymbol{G}\cdot\Delta\boldsymbol{r}\end{aligned} \tag{29}$$

with $\boldsymbol{G} = \nabla B_{gz}$, where the concomitant component perpendicular to $\boldsymbol{B}_0$ is neglected.

However, in a low-magnetic field such as the Earth's magnetic field, we encounter fundamental limits in circumstances in which the static magnetic field is not sufficiently strong to truncate unwanted concomitant components of the applied gradient fields. This limitation affects the attainable optimal image fidelity and resolution most prominently in low-field imaging. Based on this approximation, in a weak main magnetic field we can only employ a weak magnetic field gradient, and the spins may not accumulate measurable signal dephasing during the interval between the gradient pulses. Therefore, an understanding of the effect of a non-uniform magnetic field of strength equal or greater than that of the main magnetic field is needed to take advantage of the full potential of NMR in the low-magnetic fields.

4.1. Spin echo

Hahn's spin echo with a sequence of a π-pulse in between two adiabatically imposed non-uniform magnetic field pulses is described by the time evolution

$$U_j(t) = U_{j2}U_\pi U_{j1} \tag{30}$$

acting on the spins in the precessing state. The operator $U_\pi = \mathrm{e}^{\mathrm{i}\pi I_{jx}}$ has the effect of rotating all *z*- and *y*-spin components lying to the right of it by 180°. It therefore results in a change of the sign of the effective frequency in U_{j1}. After factorization we can write

$$U_j(t) = U_\pi U^*_{j2} U_{j1} \tag{31}$$

with U_{j2} transformed into the tilted frame as

$$U^*_{j2} = \mathrm{e}^{-\mathrm{i}\int_0^t \omega_{\mathrm{tot}}(t', \boldsymbol{r}_j) I_{jz}\,\mathrm{d}t'} \tag{32}$$

Multiplied operators $U^*_{j2}U_{j1}$ contain only the *z*-component of the spin variable and can be merged into a single operator for which time runs from the beginning to the end of the sequence as

$$U_j(t) = U_\pi U^*_{j2} U_{j1} = U_\pi U_{gj}(t) \tag{33}$$

with

$$U_{gj}(t) = \mathrm{e}^{\mathrm{i}\int_0^t \omega_{\mathrm{eff}}(t', \boldsymbol{r}_j) I_{jz}\,\mathrm{d}t'} \tag{34}$$

where ω_{eff} is ω_{tot}, which changes sign after the π-pulse. For the ordinary Hahn's spin echo the effective precession frequency [65,66] is defined as

$$\omega_{\mathrm{eff}}(\boldsymbol{r}_j, t) = \begin{cases} \omega_{\mathrm{tot}}(\boldsymbol{r}_j, t), & 0 < t < \frac{\tau}{2} \\ -\omega_{\mathrm{tot}}(\boldsymbol{r}_j, t), & \frac{\tau}{2} < t < \tau \end{cases} \tag{35}$$

if we assume that the π-pulse is applied at time $\frac{\tau}{2}$ and that at this time the non-uniform magnetic field is zero.

Eq. (30) can be generalized for sequences with multiple π-pulses

$$U_j(t) = U_{jn}U_\pi U_{j(n-1)}U_\pi U_{j(n-2)}\ldots U_\pi U_{j2}U_\pi U_{j1} = U^{n-1}_\pi U_{gj}(t) \tag{36}$$

where ω_{eff} in $U_{gj}(t)$ is ω_{tot} which changes sign after each π-pulse.

5. Signal acquisition

Free precession of the spin system is observed via the voltage induced in a coil wound around the sample. The signal of variable magnetization $\boldsymbol{M}(t)$ is given by

$$E(t) = -\int \frac{\mathrm{d}}{\mathrm{d}t}[\boldsymbol{M}(t,\boldsymbol{r})\cdot\boldsymbol{S}(\boldsymbol{r})]\mathrm{d}V. \tag{37}$$

where the induced signal also depends on the position of the magnetic dipole inside the coil. By the reciprocity theorem, the coil sensitivity is characterized by the ratio $\boldsymbol{S} = \boldsymbol{B}_r(\boldsymbol{r})/i_c$ where $\boldsymbol{B}_r$ is the virtual field induced by the coil carrying a virtual current i_c at the location of a magnetic dipole. For a long solenoid, the sensitivity is approximately uniform and given by

$$S = \frac{\mu_0 N}{l} \tag{38}$$

where N is the number of turns and l is the solenoid's length, while in general for finite coils $\boldsymbol{B}_r$ is not uniform and the sensitivity depends on the position of the spin within the coil. For a coil with its axis along the x-axis, the induced emf can be expressed by the density matrix as

$$E(t) = -\hbar\gamma\frac{\mathrm{d}}{\mathrm{d}t}\sum_j Tr[\rho(t)I_{jx}S_x(\boldsymbol{r}_j)] \tag{39}$$

where the time evolution of $\rho(t)$ depends on the spin interactions in the interval between the formation of magnetization and the time of signal acquisition. In addition to interactions with external fields, the interactions also include the spin–spin interaction H_{ss} and the spin–lattice interaction H_L. Factorization of the evolution operator with respect to H_L

$$U(t) = U_L(t)U_s(t) \tag{40}$$

leads to the expression

$$E(t) = -\hbar\gamma\frac{\mathrm{d}}{\mathrm{d}t}\sum_j Tr\{\rho_L\rho_{sj}(t)I_{jx}\ S_x[\boldsymbol{r}_j(t)]t\} \tag{41}$$

with

$$\rho_{sj}(t) = -\beta\hbar\gamma\sum_j B_m[\boldsymbol{r}_j(0)]U_{sj}[t,\boldsymbol{r}_j(t)]I_{jx}U_{sj}[t,\boldsymbol{r}_j(t)]\mathrm{e}^{-t/T_1} \tag{42}$$

in which the spin location depends on time due to the spin motion, and where all spin non-magnetic interactions result in magnetization decay with the rate $1/T_1$.

By assuming that during the acquisition period spins precess in the constant magnetic field B_a applied along the z-axis (it could be the Earth's magnetic field B_0 or, in the case of MRI, the inhomogeneous magnetic field comprised of the readout magnetic gradient and the uniform magnetic field), then the induction signal of spins precessing with the frequency $\omega_a[\boldsymbol{r}_j(t)] = \gamma\ B_a[\boldsymbol{r}_j(t)]$ can be generalized as

$$E(t) = \beta\hbar^2\gamma^2 Tr_s I_x^2\sum_j\left\langle\omega_a[\boldsymbol{r}_j(t)]\ B_m[\boldsymbol{r}_j(0)]\ S_x[\boldsymbol{r}_j(t)]\mathrm{e}^{\mathrm{i}\theta_j(t)}\right\rangle \times \mathrm{e}^{\mathrm{i}\omega_a[\boldsymbol{r}_j(t)](t-t_a)-(t-t_e)/T_2-t/T_1} \tag{43}$$

with $\langle\ldots\rangle = Tr_L(\rho_L\ldots)$ and $\theta_j(t) = \int_{t_e}^{t}\omega_{eff}(t',\boldsymbol{r}_j(t'))\,\mathrm{d}t'$. Here t_e is the time of spin excitation, while t_a is the start of acquisition. Spin–spin interactions and interactions with internal magnetic fields are embraced in the relaxation time T_2.

6. Flow and diffusion by spin echo

The determination of molecular migration by NMR has a long history [67–72]. By labeling the spin-bearing molecules by their precession in a non-uniform magnetic field $\boldsymbol{B}_g$, the method is non-destructive and non-invasive and thus attractive for studying molecular random migrations in various systems. Particle motion across the non-uniform magnetic field causes dephasing of spins that leads to attenuation of the signal. The attenuation depends on the strength of the non-uniform magnetic field, its duration, and the rate of particle motion.

The spin relaxation limits the interval of gradient application and in the study of slow migration a strong non-uniform magnetic field has to be applied. The strength of the non-uniform field may be greater than that of the weak Earth's magnetic field, preventing the usual magnetic field gradient approximation because the concomitant components of the non-uniform magnetic field cannot be neglected. However, in the following we will show that a certain geometry of the gradient coil cancels the effect of the concomitant field component in the diffusion attenuation of the spin echo at any strength of the gradient field.

With relaxation in Eq. (43) neglected, the motion of spin bearing particles is encoded in the spin echo amplitude and phase via the magnetic field inhomogeneity

$$\langle\mathrm{e}^{\mathrm{i}\theta_j(t)}\rangle = \left\langle\mathrm{e}^{\mathrm{i}\int_{t_e}^{t}\omega_{eff}(t',\boldsymbol{r}_j(t'))\mathrm{d}t'}\right\rangle \tag{44}$$

and in its amplitude via the spatial variation of initial magnetization and the spatially dependent sensitivity of the receiving coil

$$\langle\omega_a[\boldsymbol{r}_j(t)]\ B_m[\boldsymbol{r}_j(0)]\ S_x[\boldsymbol{r}_j(t)]\rangle \tag{45}$$

This means that various inhomogeneities can provide information about flow or diffusion. Here, we mostly deal with motion which is encoded in the spin echo phase, but it is important to note that RF gradients can also be used for measurement of particle migration, not only as dephasing by the RF inhomogeneity in the rotating frame, but also as a correlation between the initial distribution of excited spins and the coil sensitivity to their location at the time of detection, as shown in [73–75].

A small displacement of the jth spin from its initial position, $\boldsymbol{r}_j(t) = \boldsymbol{r}_{j0} + \Delta\boldsymbol{r}_j(t)$, changes the spin precession as

$$\omega_{eff}[\boldsymbol{r}_j(t),t] = \omega_{eff}(\boldsymbol{r}_{0j},t) + \Delta\boldsymbol{r}_j(t)\cdot\nabla[\omega_{eff}(\boldsymbol{r}_{0j},t)] \tag{46}$$

By per-partes integration we obtain the phase of spins at the peak of the spin-echo signal [65,66]

$$\theta_j(\tau) = -\int_0^\tau \boldsymbol{q}_j(\boldsymbol{r}_{j0},t)\cdot\boldsymbol{v}_j(t')\mathrm{d}t' \tag{47}$$

where $\boldsymbol{v}_j$ is the particle velocity and

$$\boldsymbol{q}(\boldsymbol{r}_{j0},t) = \int_0^t \nabla[\omega_{eff}(\boldsymbol{r}_{0j},t')]\,\mathrm{d}t' \tag{48}$$

In Eq. (47) we assume that the applied sequence of a non-uniform magnetic field and π-pulses refocuses the spin phase at time τ, so that

$$\int_0^\tau \omega_{eff}(\boldsymbol{r}_{j0},t)\mathrm{d}t = 0 \tag{49}$$

and according to the definition in Eq. (48), also

$$\boldsymbol{q}(\boldsymbol{r}_{j0},\tau) = 0 \tag{50}$$

The resulting signal of the gradient spin echo is a sum of the spin contributions

$$E(\tau) = E_0\sum_j\left\langle\mathrm{e}^{-\int_0^\tau\boldsymbol{q}(\boldsymbol{r}_{j0},t)\cdot\boldsymbol{v}_j(t')\mathrm{d}t'}\right\rangle \tag{51}$$

where the particle velocity is encoded in the temporal average of the spin phase.

For a sequence of two short gradient pulses (SPGSE), the method of averaged propagator [76,77] is commonly used to evaluate the mean of spin-echo phase fluctuations. The method works for

very narrow gradient pulses (width δ), and with the requirement that the spin dephasing $\boldsymbol{q} = \gamma \boldsymbol{G}\delta$ can be varied over a broad interval of amplitudes. Because the strength of the applied non-uniform field is limited, this method is not useful in low field NMR.

Another method to average the phase factor in Eq. (51) is the Gaussian phase approximation or the cumulant expansion of the averaged spin phase to the second term. The method stems from the theory of stochastic processes of a random variable $v(t)$ which is characterized by a functional of identical form as the spin-echo signal in Eq. (51). The characteristic functional, which completely describes the stochastic process, can be expanded into the cumulant series as shown in Appendix III. According to this theory, the average of spin echo dephasing due to random motion in the non-uniform magnetic field, can be approximated by the first two terms of the cumulant series if the spin diffusive displacement is short compared to the wavelength of the spin phase grating created by the applied gradient [78]. Neglecting the relaxation, it gives the echo signal as a superposition of signals induced by a large number of spins in the form

$$E(\tau) = E_0 \sum_j \mathrm{e}^{\mathrm{i}\varphi_j(\tau)-\beta_j(\tau)} \tag{52}$$

where the signal phase

$$\varphi_j(\tau) = \int_0^\tau \boldsymbol{q}_j(\boldsymbol{r}_{j0}, t)\cdot\langle \boldsymbol{v}_j(t')\rangle \mathrm{d}t' \tag{53}$$

includes the averaged spin velocity $\langle \boldsymbol{v}_j(t)\rangle$ such as flow, while the signal attenuation [79]

$$\beta_j(t) = \frac{1}{2}\int_0^t \mathrm{d}t_1 \int_0^t \mathrm{d}t_2 \boldsymbol{q}(\boldsymbol{r}_{j0}, t_1)\cdot\langle \delta\boldsymbol{v}_j(t_1)\ \delta\boldsymbol{v}_j(t_2)\rangle \boldsymbol{q}(\boldsymbol{r}_{j0}, t_2) \tag{54}$$

includes the autocorrelation function of deviation from the averaged velocity $\delta\boldsymbol{v}(t) = \boldsymbol{v}(t) - \langle \boldsymbol{v}(t)\rangle$.

In general form the time correlations between the components of a particle's velocity are represented by a tensor

$$\mathscr{D}(t_1, t_2) = \frac{1}{2}\begin{bmatrix} \langle \delta v_x(t_1)\delta v_x(t_2)\rangle & \langle \delta v_x(t_1)\delta v_y(t_2)\rangle & \langle \delta v_x(t_1)\delta v_z(t_2)\rangle \\ \langle \delta v_y(t_1)\delta v_x(t_2)\rangle & \langle \delta v_y(t_1)\delta v_y(t_2)\rangle & \langle \delta v_y(t_1)\delta v_z(t_2)\rangle \\ \langle \delta v_z(t_1)\delta v_x(t_2)\rangle & \langle \delta v_z(t_1)\delta v_y(t_2)\rangle & \langle \delta v_z(t_1)\delta v_z(t_2)\rangle \end{bmatrix} \tag{55}$$

so that the attenuation (Eq. (54)) can be written as

$$\beta_j(t) = \int_0^t \mathrm{d}t_1 \int_0^t \mathrm{d}t_2 \boldsymbol{q}(\boldsymbol{r}_{j0}, t_1)\cdot\mathscr{D}_j(t_1, t_2)\boldsymbol{q}(\boldsymbol{r}_{j0}, t_2) \tag{56}$$

In the case of isotropic molecular random walk where the tensor has the form

$$\mathscr{D}(t_1 - t_2) = D\begin{bmatrix} 1 & 0 & 0 \\ 0 & 1 & 0 \\ 0 & 0 & 1 \end{bmatrix}\delta(t_1 - t_2) \tag{57}$$

and D is the self-diffusion coefficient, Eq. (54) is simplified into

$$\beta_j(t) = D\int_0^t |\boldsymbol{q}(\boldsymbol{r}_{j0}, t')|^2 \mathrm{d}t'. \tag{58}$$

This resembles Torrey's expression [72] but there are notable differences. In the classical approach the perpendicular component of the magnetic field is neglected, and migration along the gradient of the component parallel to the main field is responsible for the signal attenuation. Here, all components of the magnetic field play a part. Thus, $\boldsymbol{q}(\boldsymbol{r}_{j0}, t)$ includes the gradient of the Larmor frequency ω_{eff}, which is related to the magnetic field by

$$\nabla\omega_{\mathrm{eff}} = \gamma\frac{B_x\nabla B_x + B_y\nabla B_y + B_z\nabla B_z}{|\boldsymbol{B}|} \tag{59}$$

By taking into account $\nabla\times\boldsymbol{B} = 0$ this expression becomes

$$\nabla\omega_{\mathrm{eff}} = \gamma\frac{(\boldsymbol{B}\cdot\nabla)\boldsymbol{B}}{|\boldsymbol{B}|} \tag{60}$$

Thus, the gradient of the effective Larmor frequency is proportional to the change of the magnetic field along its direction. This is historically called "the line gradient of the magnetic field" (LGMF). The main difference from Torrey's approximation is that the spin dephasing results from the molecular motion along the gradient of total magnetic field magnitude and not only component parallel to B_0.

For quadrupolar gradient coils with their axis perpendicular to B_0, the total magnetic field can be approximated as $\boldsymbol{B} = (-Gz, 0, -Gx + B_0)$ in a wide region between the coils. Here, G describes the non-uniformity of the magnetic field near the origin of the coordinate system and, in the usual gradient approximation where only the derivative of the z component is used, corresponds with the gradient in the x direction. LGMF is

$$\nabla|\boldsymbol{B}| = G\frac{(-Gx + B_0, 0, Gz)}{|\boldsymbol{B}|} \tag{61}$$

with the absolute value

$$|\nabla|\boldsymbol{B}||^2 = G^2 \tag{62}$$

Self-diffusion attenuation follows from Eq. (58) as

$$\ln\frac{E(t)}{E_0} = \gamma^2 D\int_0^t \left|\int_0^u G(t')\mathrm{d}t'\right|^2 \mathrm{d}u \tag{63}$$

In this case the formula is identical to Torrey's result. This is not true, however, for the non-uniform magnetic field of reversed Helmholtz coils. We show the results of this calculation in Appendix.6 where we prove that Torrey's formula is unsuitable for self-diffusion measurement when $B_g(\boldsymbol{r}_j, t) \geqslant B_0$.

It turns out as a rule that Torrey's formula holds only if non-zero components of the strong non-uniform magnetic field have the same first derivatives. Thus, the spin-echo method imposes certain requirements regarding the symmetry of the applied non-uniform magnetic field.

6.1. Echo attenuation in the frequency domain

As shown above, Hahn's echo is an effective method of measuring a diffusion coefficient – or the time integral of the velocity autocorrelation function (VAF). However, if we translate the expression for the echo attenuation to the frequency domain, we can realize the potential of modulated gradient spin echo (MGSE) for measurement of the diffusion spectrum, defined as the Fourier transform of VAF

$$\mathscr{D}(\omega) = \frac{1}{2}\int_{-\infty}^{\infty}\langle \boldsymbol{v}(\tau)\boldsymbol{v}(0)\rangle \mathrm{e}^{\mathrm{i}\omega\tau}\,\mathrm{d}\tau \tag{64}$$

The echo attenuation $\beta(\boldsymbol{r}_{j0})$ can be expressed in terms of $\boldsymbol{q}(\boldsymbol{r}_{j0}, \omega)$, the Fourier transform of the phase factor,

$$\boldsymbol{q}(\boldsymbol{r}_{j0}, \omega) = \int_0^\tau \boldsymbol{q}(\boldsymbol{r}_{j0}, t)\mathrm{e}^{\mathrm{i}\omega t}\,\mathrm{d}t = \int_{-\infty}^{\infty}\boldsymbol{q}(\boldsymbol{r}_{j0}, t)\mathrm{e}^{\mathrm{i}\omega t}\,\mathrm{d}t \tag{65}$$

(the integration can be extended to infinity, because the phase factor can be set to 0 outside the interval $(0, \tau)$) as

$$\beta(\boldsymbol{r}_{j0}) = \frac{1}{\pi}\int_{-\infty}^{\infty}\mathrm{d}\omega\boldsymbol{q}(\boldsymbol{r}_{j0}, -\omega)\cdot\mathscr{D}(\omega)\boldsymbol{q}(\boldsymbol{r}_{j0}, \omega) \tag{66}$$

For isotropic diffusion this simplifies to

$$\beta_j = \frac{1}{\pi}\int_0^\infty D_j(\omega)|\boldsymbol{q}_j(\omega)|^2\,\mathrm{d}\omega \tag{67}$$

and for Brownian diffusion (VAF with a very short correlation time) it can be further simplified to

$$\beta_j = \frac{1}{\pi}D_j(0)\int_0^\infty |\boldsymbol{q}_j(\omega)|^2\,\mathrm{d}\omega \tag{68}$$

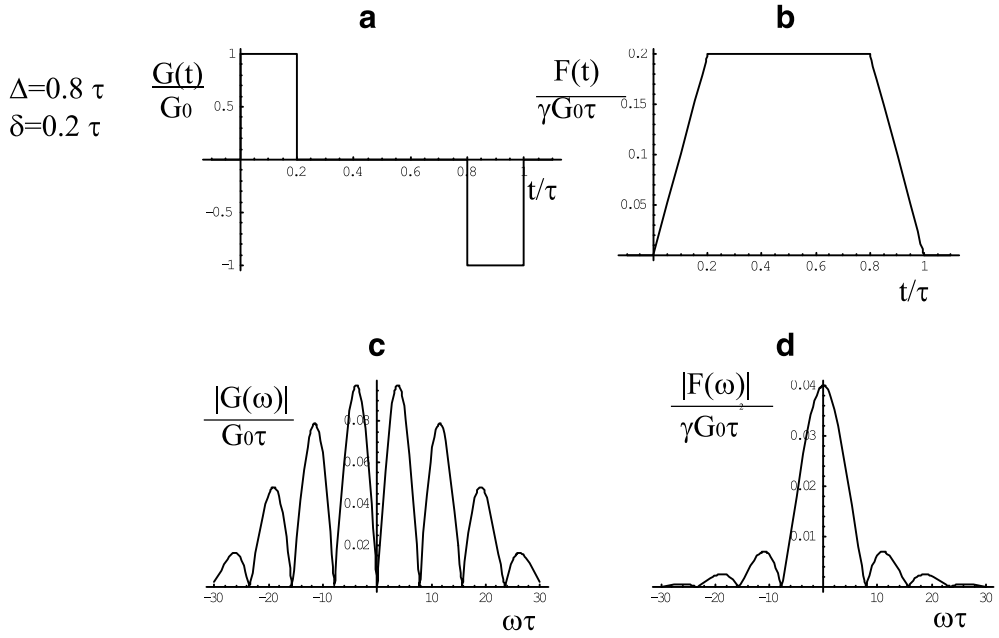

Fig. 5. Time dependence of (a) the effective gradient field, (b) the phase factor and their Fourier transforms (c) and (d) for a PGSE sequence.

which can be translated to Torrey's formula [72]

$$\beta_j = D_j(0)\int_0^\tau |\boldsymbol{q}_j(t)|^2\,\mathrm{d}t \tag{69}$$

using Parceval's identity. Here, the index j denotes the subensemble at $\boldsymbol{r}_{j0}$.

6.2. Modulated gradient spin echo

In this section, we will use the uniform gradient approximation $B_g \ll B_0$ so

$$\nabla B_z = \nabla(B_0 + \boldsymbol{G}\cdot\boldsymbol{r}) = \boldsymbol{G} \tag{70}$$

and the phase factor is

$$\boldsymbol{q}(t) = \gamma\int_0^t \boldsymbol{G}(t')\,\mathrm{d}t' \tag{71}$$

The Fourier transform of the phase factor can be expressed by $\boldsymbol{G}(\omega) = \int_{-\infty}^{\infty}\boldsymbol{G}(t)\mathrm{e}^{\mathrm{i}\omega t}\,\mathrm{d}t$, the Fourier transform of the gradient, as

$$\boldsymbol{q}(\omega) = \mathrm{i}\gamma\frac{\boldsymbol{G}(\omega)}{\omega} \tag{72}$$

As a demonstration, we will discuss the pulsed gradient spin echo (PGSE) sequence. In this method of measuring the diffusion coefficient, two δ long gradient pulses Δ apart are interspersed by a π-pulse at the time $\tau/2$ after excitation and the effective gradient (Fig. 5a) can be described by

$$G(t) = G_0(H[t] - H[t-\delta] - H[t-\Delta] + H[t-\Delta+\delta]) \tag{73}$$

and the corresponding phase factor (Fig. 5b) is

$$q(t) = \gamma G_0(t(H[t] - H[t-\delta]) + \delta(H[t-\delta] - H[t-\Delta]) + (\Delta+\delta - t)(H[t-\Delta] - H[t-\Delta-\delta])) \tag{74}$$

$H(t)$ is a unit step function. The gradient Fourier transform (Fig. 5c) is

$$G(\omega) = -4\mathrm{i}G_0\mathrm{e}^{\mathrm{i}\omega\delta/2}\mathrm{e}^{\mathrm{i}\omega\Delta/2}\frac{\sin\frac{\omega\delta}{2}\sin\frac{\omega\Delta}{2}}{\omega} \tag{75}$$

and the spectrum of the phase factor (Fig. 5d) is

$$q(\omega) = 4\gamma G_0\mathrm{e}^{\mathrm{i}\omega\delta/2}\mathrm{e}^{\mathrm{i}\omega\Delta/2}\frac{\sin\frac{\omega\delta}{2}\sin\frac{\omega\Delta}{2}}{\omega^2} \tag{76}$$

For the spin motion described by a constant diffusional spectrum (Brownian motion), the echo attenuation is the well-known expression

$$\beta = \gamma^2 G_0^2 D\delta^2(\Delta - \delta/3) \tag{77}$$

Another example of an MGSE sequence is described in Section 9.

7. Signal-to-noise ratio

The induced signal of a completely filled solenoid is

$$E(t) = \mu_0\omega_0 M_0 V N_l \mathrm{e}^{\mathrm{i}\omega_0 t}\mathrm{e}^{-t/T_2^*}$$

where $\omega_0 = \gamma B_0$ is the Larmor frequency, N_l the number of turns per unit length of the receiving coil, V the sample volume and T_2^* the effective spin relaxation time. M_0 is the initial magnetization (magnetic moment density), obtained from Curie's law which for protons gives

$$M_0 = n\beta\gamma^2\hbar^2 B_\mathrm{m}/4$$

and is approximated here, as well as the coil sensitivity, as uniform over the sample. n is the number of protons per unit volume. The signal and the noise are Fourier transformed after application of an optimum filter and the resulting spectral line has an S/N

$$\frac{S}{N} = \frac{E(0)\sqrt{T_2^*/2}}{\sqrt{\mathrm{d}\langle U_n^2\rangle/\mathrm{d}\nu}}$$

Noise can be conveniently expressed as the Johnson noise $U_n = \sqrt{4kT\,\mathrm{d}\nu R}$ where R is the dominant source of resistance. In the case of a low-magnetic field, the resistance is caused by Ohmic resistance of the receiving coil $R_\mathrm{L} = \rho_\mathrm{c}N_\mathrm{L}2\pi r/S_\mathrm{c}$, where ρ_c is the specific resistance of the conducting wire with a cross-section S_c, N_L is the number of receiver coil turns and r the radius of the coil. At high rf frequencies the skin effect increases the effective coil resistance which, however, is still negligible compared to the inductive resistance of the sample $R_\mathrm{H} = \pi\omega_0^2\mu_0^2 N_\mathrm{H}^2 r^3/60\rho_s$, where a spherical phantom of radius r inside a solenoidal coil of the same radius and half-

height is considered, ρ_s is the sample specific resistance and N_H is the number of turns of the high-field receiving coil.

If we compare the S/N in low and high field for samples of equal volume, the result is

$$\frac{(S/N)_L}{(S/N)_H} = \frac{\omega_{0L} N_L M_{0L} \sqrt{T^*_{2L} R_H}}{\omega_{0H} N_H M_{0H} \sqrt{T^*_{2H} R_L}}$$

or, with the above defined resistances

$$\frac{(S/N)_L}{(S/N)_H} = \frac{\mu_0 \omega_{0L} r M_{0L} \sqrt{N_L S_c T^*_{2L}}}{M_{0H} \sqrt{120 \rho_s \rho_c T^*_{2H}}}$$

For comparison with a spherical sample of $r = 5$ cm, $S_c = 3$ mm^2, $N = 3000$, $\nu_{0L} = 2$ kHz, $\rho_s = 0.5$ Ωm, and $\rho_c = 1 \times 10^{-8}$ Ωm, the relative sensitivity of the EFNMR experiment is

$$\frac{(S/N)_L}{(S/N)_H} \approx 0.1 \frac{\sqrt{T^*_{2L}} m_{0L}}{\sqrt{T^*_{2H}} m_{0H}}$$

This result shows that in spite of the fact that the Earth's magnetic field is about five orders of magnitude weaker than the field usually used for NMR imaging, the S/N is only a few times lower than that in the high field, under the assumption that magnetization in the pre-magnetization field m_{0L} is about the same as the magnetization m_{0H} in the high field [80]. If no attention is paid to reducing the surrounding electromagnetic noise (shielding, gradiometric coils), the S/N is easily degraded by an order of magnitude. In fact electromagnetically polluted surroundings contribute the most to the noise in EFNMR.

8. EFNMR measuring system

Work on the Ljubljana EFNMR system started in the early 1980s. In the beginning the system consisted only of a pre-magnetizing coil, which served as the detection coil as well, and two gradient coils – one with the gradient parallel to the symmetry axis of the pre-magnetizing coil and used for slice selection, and the other with its gradient parallel to the Earth's magnetic field for position encoding in free induction decay, as used in the projection reconstruction technique. The spatial distribution of spins was determined by rotating the sample. An aluminum box was used for electromagnetic shielding. The system was later moved outside the city where better field stability and less noise was attained. A dedicated coil is used for pre-magnetization and shielding during the detection period. Two gradiometric coils support the shield. Besides pre-magnetization, a typical NMR experiment consists of a preparation period (excitation of magnetization with an oscillating magnetic field and phase encoding with magnetic field gradients) and a detection period. In order to do suitable pulse experiments together with signal phase detection, a separate reference spectrograph is used to provide an independent clock (oscillator) with the period determined by the actual Earth's magnetic field.

The scheme of the components necessary to perform NMR imaging experiments is shown in Fig. 6. Uniaxial coils (detection, three gradient, AF, and pre-magnetizing) constitute the core of the system (Fig. 7).

In the main spectrograph, the pre-magnetizing magnetic field of 60 mT is switched off adiabatically, leaving magnetization aligned along B_0. Thus, the orientation of the pre-magnetizing coil is not important. The symmetry axis of the pre-magnetizing coil lies horizontally and is perpendicular to the Earth's magnetic field. The axis is parallel with that of the detection coil enabling easy access to the sample area. When grounded during the detection period, the pre-magnetizing coil acts as a shield against external AF interferences.

Magnetization is excited by AF pulses produced by a solenoid on the inner side of the pre-magnetizing coil. It is much larger than the detection coil so the AF field is uniform across the sample region. The coil is tuned to the Larmor frequency. On our system typical duration of a $\pi/2$-pulse is a few Larmor periods (about 5 ms). The periodic input to the AF coil comes from the reference spectrometer. In strong field NMR this signal is provided by a stable frequency oscillator. The envelope of the AF signal can be controlled thus enabling soft excitation pulses.

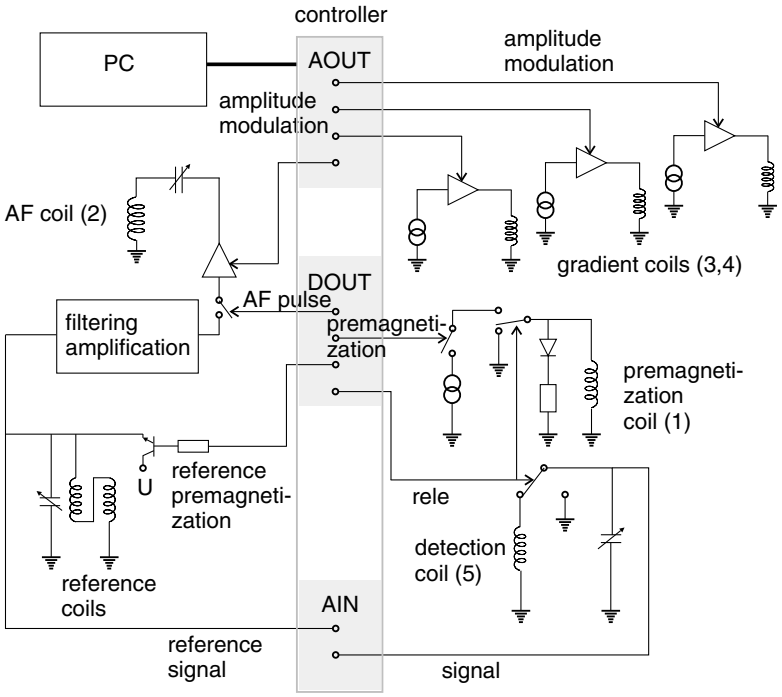

Fig. 6. Block diagram of the Ljubljana EFNMR system. The core features of the system are the uniaxial coils: detection, three gradient, AF, and pre-magnetizing coils, controlled by a homemade pulse programmer connected to a PC. The reference coil provides the AF signal needed for pulse generation and quadrature detection.

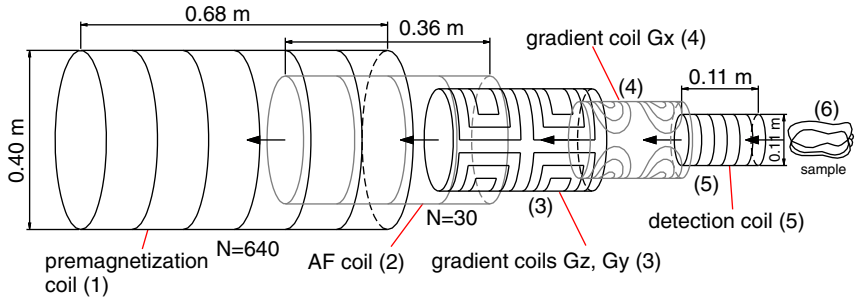

Fig. 7. The coils of the system; the outermost coil is the pre-magnetizing coil and the detection coil is at the center. The AF and gradient coils are located in between these two. All coils are centered at the same point. The coils are shown in a pull-out side-view for clarity.

After excitation, the magnetization can be manipulated with additional AF pulses and magnetic field gradients produced by the gradient coils. The frequency and the phase of the signal are controlled by three orthogonal magnetic field gradients. Three gradient coils produce quadrupolar magnetic fields with components parallel to the Earth's field changing linearly in three orthogonal directions. The gradient coils have low inductances in order to minimize transients.

The gradients in directions perpendicular to the symmetry axis of the detection coil (z and y gradient) are produced by quadrupolar coils with a symmetry axis along x. The wires are distributed to produce a current density on the surface of the cylinder that varies as $\sin 2\varphi$ for the z gradient and as $\cos 2\varphi$ for the y gradient; φ is the polar angle measured from the z axis. A continuous distribution is mimicked by changing the distance between the wires. The magnetic fields produced by these two coils are given by

$$\boldsymbol{B}_{gz} = (0, -Gy, Gz)$$
$$\boldsymbol{B}_{gy} = (0, Gz, Gy) \tag{78}$$

with a gradient per unit current $G/I = 2 \times 10^{-4}$ T/Am.

The x gradient is produced by a quadrupolar coil with the distribution of wires determined by the target field method [81,82]. In the first approximation the field produced by this coil is

$$\boldsymbol{B}_{gx} = (Gz, 0, -Gx) \tag{79}$$

with the gradient per unit current $G/I = 4.25 \times 10^{-4}$ T/A m. The span of the linear gradient region is 11 cm.

The NMR signal in high-magnetic field is usually detected by low-inductance coils (small number of turns) because the coils must be tuned to the high Larmor frequency. Coils with a small number of turns produce low thermal noise which increases with the fourth root of the Larmor frequency (due to the skin effect). Sample induced thermal noise (caused by dissipation of induced currents) increases linearly with the Larmor frequency. In a strong magnetic field the sample-induced thermal noise dominates the coil's thermal noise. In our case, detecting coils with a high number of turns can be successfully used because the signal frequency is low. In the Earth's magnetic field sample-induced noise can be neglected and even the coil thermal noise is often smaller than the noise induced by the background electromagnetic field, unless the experiment is performed in an AF shielded environment. To some extent rapid interferences in the magnetic field, usually caused by urban activities (railway, electrical network, distant storms, etc.), can be reduced using gradiometric coils or shield coils. A grounded polarizing coil is employed as a shield [83]. The detecting coil is a solenoid (with 6000 turns) placed coaxially with the polarizing coil and perpendicular to Earth's magnetic field. The large number of turns enhances the signal and the turns are wound in six sectors to minimize the self-capacitance of the coil. The coil is connected to the preamplifier only during signal acquisition. The quality of the coil is deliberately lowered to enable the detection of the signal from a 200 Hz bandwidth. A wider bandwidth receiving coil does not require sharp tuning to the signal frequency.

Besides the signal amplitude, a knowledge of both the phase and the frequency of the signal is necessary in imaging. The fluctuations in magnetic field affect the Larmor frequency and these fluctuations hinder the detection of the phase and frequency of the signal. Random phase changes of the signal also attenuate the averaged signal. The phase and the frequency of the signal are controlled by AF pulses and magnetic field gradients, but in order to determine the phase at a given time, the exact time variation of the Larmor frequency should be known. In quadrature detection, common practice is to use a harmonic signal generated by a stabilized oscillator and to stabilize the static field by shim coils controlled by the signal from an appropriate probe (spin-lock signal) whenever phase stability is an issue. This method is inadequate in our case; the problem is the temporal instability of the Earth's magnetic field. Since scanning is inherently slow because of the pre-magnetization period, changes in magnetic field are inevitable. Accurate detection of the signal phase, using a fixed-frequency reference oscillator, is impossible and active shimming of slow field fluctuations is practically challenging. This problem is circumvented by using a reference oscillating signal provided by a separate NMR spectrometer – the "reference coils". The spectrometer, placed a short distance (20 m) from the imaging coils, experiences similar B_0 but does not disturb the measurements. It consists of two solenoids placed next to each other; their symmetry axes are perpendicular to B_0 (parallel to the symmetry axis of the detection coil). Each coil contains a water-filled container. The coils are connected in series but oriented in a gradiometric arrangement to improve S/N. The reference coils perform two tasks: they are used for pre-magnetization of the sample and to detect the free induction decay. Magnetization is induced in the direction perpendicular to B_0 (along the symmetry axes of the coils). The polarizing current is slightly undercritically damped upon the source switch-off. As the current in the coils decays after a few oscillations, the magnetization remains in the plane perpendicular to B_0 and a free induction signal is induced with no need for AF pulses. The pre-magnetizing field of the reference coils is switched off before the pre-magnetizing field of the imaging coils since the reference signal is needed for the AF excitation pulse. The reference signal s_r is given by

$$s_r = s_{0r} \sin(\omega_0 t + \omega_f t + \varphi_f + \varphi_r) \tag{80}$$

where s_{0r} is the amplitude of the signal (can be set to 1, since its source is saturated amplifier and the only importance of the reference signal are its phase and frequency), ω_0 is the average Larmor frequency, ω_f represents the fluctuations in the magnetic field, φ_f is a random phase induced by magnetic bursts, and φ_r is the phase of the undisturbed reference signal and can be set to zero. The signal shifted in phase by $\pi/2$, required for quadrature detection, is generated by a phase shifter. If the signal s_m from a voxel is

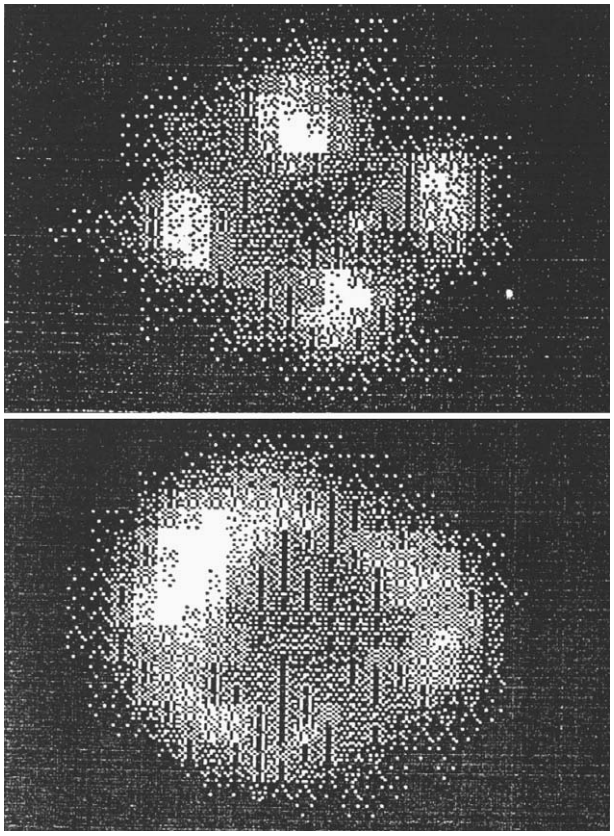

Fig. 8. The first images taken by NMR in the Earth's magnetic field: Top, four water-filled tubes 1 cm^3 each; bottom, a pumpkin cross-section of 20 cm [16].

$$s_m = s_{0m}\sin(\omega_0 t + \omega_f t + \omega_m t + \varphi_f + \varphi_m) \tag{81}$$

where $\omega_m t$ is the phase generated by the magnetic field gradient applied during signal acquisition (readout gradient) and φ_m is the phase of the signal generated by the gradient applied during magnetization manipulation (phase gradient) and we assume that the field fluctuations at the sample and reference coils are the same, quadrature detection gives the real and imaginary parts s_r and s_i of the signal

$$s_r = \frac{1}{2}s_{0m}s_{0r}\cos(\omega_m t + \varphi_m - \varphi_r) \tag{82}$$

$$s_i = \frac{1}{2}s_{0m}s_{0r}\sin(\omega_m t + \varphi_m - \varphi_r) \tag{83}$$

The unwanted phase and frequency fluctuations cancel out.

9. Experimental overview

The NMR studies performed on the Ljubljana system include diffusion measurements [56], imaging [11–16,21], flow measurements combined with imaging of flow distribution [57], T_1 and T_2 measurements and contrast enhancement in imaging [9], imaging of diffusion distribution [58], natural convection [59], and other more specialized unpublished experiments such as slice selection specific measurements [84].

For most imaging experiments on the new system, the spin-warp imaging technique [85] is employed, whereas in the beginning the technique of Pacard and Varian [1] combined with projection reconstruction was used. The first NMR images ever made in the Earth's magnetic field are shown in Fig. 8. The field of view is 20 cm with a resolution of 1 cm. Some newer examples are shown in Fig. 9. They show slices of some fruits. A typical scan takes of the order of an hour. With gradient coils the field of view is limited to a maximum of 30 cm, and the best resolution achieved so far is 2 mm/pixel.

Flow measurements have been performed using different techniques such as spin warp, time of flight, wash in/out described elsewhere [86–88]. Examples of flow measurements are shown in Fig. 10. The figure shows a slice profile of water flowing in cylindrical tube. From the slice profile and encoding parameters, the flow velocity can be determined.

The relaxation times for different substances have also been measured. For this purpose two new techniques for single-scan T_1 measurement were developed. The experiments are basically field-cycling experiments. The sample is pre-magnetized in a relatively strong magnetic field B_m and then adiabatically switched-off, leaving the net magnetization along B_0. A $\pi/2$-pulse creates a free-induction signal with an amplitude

$$E_1 = E_0\left[1 - \exp\left(-\frac{t_m}{T_1^m}\right)\right]\exp\left(-\frac{t_d}{T_1}\right)\exp\left(-\frac{t}{T_2}\right) \tag{84}$$

where superscript m indicates relaxation in the pre-magnetizing field and variables without an index indicate the values in the Earth's magnetic field; t_m is the duration of pre-magnetization and t_d is the interval between B_m switch-off and the excitation $\pi/2$-pulse, from which t is measured. To use the advantages of low field, more specialized weighting techniques were developed, such as technique analogous to inversion-recovery in strong field MRI. Here, two pre-magnetization periods are employed, as shown in Fig. 11a. The direction of sample magnetization is changed in the interval between the periods by a π-pulse. This technique is called *magnetization subtraction*. For this sequence, the signal amplitude is (for a long first pre-magnetization period $t_{m1} > 5T_1^m$)

$$E_2 = E_0\left\{1 - \exp\left(-\frac{t_{m2}}{T_1^m}\right)\left[1 + \exp\left(-\frac{t_1}{T_1}\right)\right]\right\}\exp\left(-\frac{t_d}{T_1}\right) \tag{85}$$

Because of the excellent B_0 homogeneity, the signal decays with a pure T_2, giving enough time to perform multiple spin manipulations in a single scan, so a gradual increase of magnetization in B_m can be observed in a single experiment, as shown in Fig. 11b. The nth amplitude of the signal after the $\pi/2$-pulse is

$$E_n = E_0(1 - E_m)E_a\frac{1 - (E_m E_a E_s)^n}{1 - E_m A_a E_s} \tag{86}$$

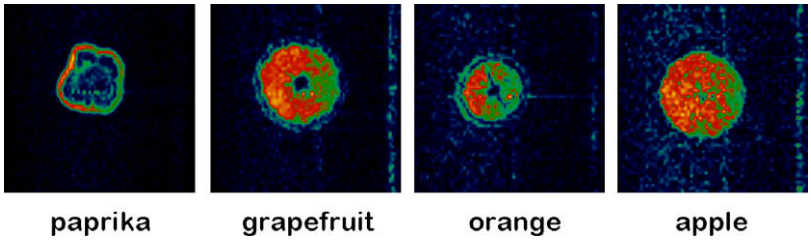

Fig. 9. Images obtained with the spin warp imaging sequence in the Earth's magnetic field: paprika, grapefruit, orange, and apple. The field of view is 15 cm with a resolution of 64 × 64 pixels. Images reprinted with permission from [21].

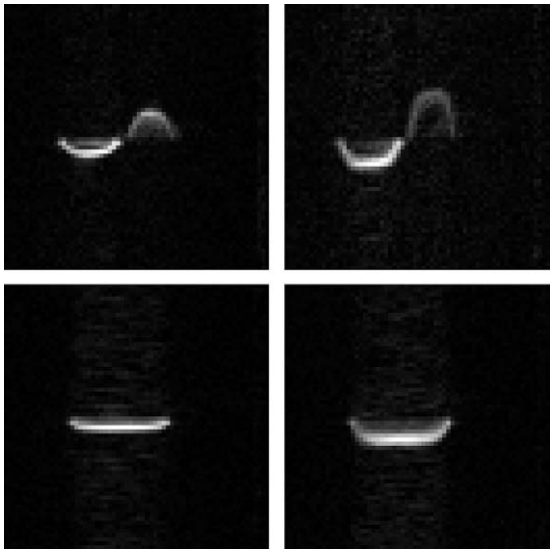

Fig. 10. An example of flow measurements. The images show deformation in a plane slice of excited water spins after the encoding time for counter-flows in two pipes (top) and flow in a single pipe (bottom).

where $E_m = \exp\left(-\frac{t_m}{T_1^m}\right)$, $E_a = \exp\left(-\frac{t_d}{T_1}\right)$, $E_s = \exp\left(-\frac{t_s}{T_2}\right)$.

The equivalent sequence for a single-scan T_1 measurement is shown in Fig. 11c. The amplitude of the nth signal, if magnetization in the Earth's field is neglected, is

$$E'_n = E_0(1 - E_m)E_a(E_s E_r)^{n-1} \tag{87}$$

where $E_r = \exp\left(-\frac{t_r}{T_1}\right)$.

The shortest measurable relaxation times are limited by the duration of the excitation pulse to some 10 ms and T_2 should be no shorter than 200 ms on the present Ljubljana system. The measurements are interesting since the results differ from those in a strong field because the relaxation is caused by field fluctuations on a different frequency scale. Likewise image contrast can be manipulated as shown in Fig. 12 of [9].

Diffusion measurements are quite simple yet specific, since B_0 is of the same order of magnitude as the gradient field. In the Earth's magnetic field the concomitant components of magnetic field cannot be neglected in certain cases, as described above and in [56,89,65,66]. Self-diffusion of different liquids was measured by the pulsed gradient spin echo [68,69,67,72,70,71] method.

We measured self-diffusion with a quadrupolar gradient coil where the effect of concomitant components on the spin-echo attenuation in the case of isotropic molecular diffusion is canceled. The magnetic field gradient was stepped from a negative to a positive value $\pm 6 \times 10^{-4}$ T/m, with the maximum non-uniform magnetic field exceeding the strength of the Earth's magnetic field in the sample. Fig. 13 shows self-diffusion measurements of water, propanol and ethanol where the amplitudes of the spin-echo fit well to Gaussian curves and confirm the validity of Torrey's formula, despite the gradient approximation violation as explained in Appendix II.

The range of diffusion constants that can be measured is limited by the finite gradient strength of 0.02 T/m (and relaxation, which limits the encoding time). However, measurements of diffusion constant distribution by spin-warp imaging preceded by a pulsed gradient spin echo (PGSE) sequence to enhance the diffusional contrast [58], as shown in Fig. 14, did unveil some unusual results. Since imaging makes the experiment quite long, we were able to observe very slow fluctuations in liquid flow induced by natural convection which appeared as an enhanced diffusion constant (Fig. 15). Usually this effect shows up only as a shift in the image phase, but not as attenuation of the signal. This effect of natural convection is described in detail by Mohorič and Stepišnik [59].

Attenuation of the spin signal due to natural convection was demonstrated in the measurement of the diffusion coefficient distribution in a propanol filled cylindrical phantom with a diameter of 10 cm using a PGSE sequence of two δ long gradient pulses of

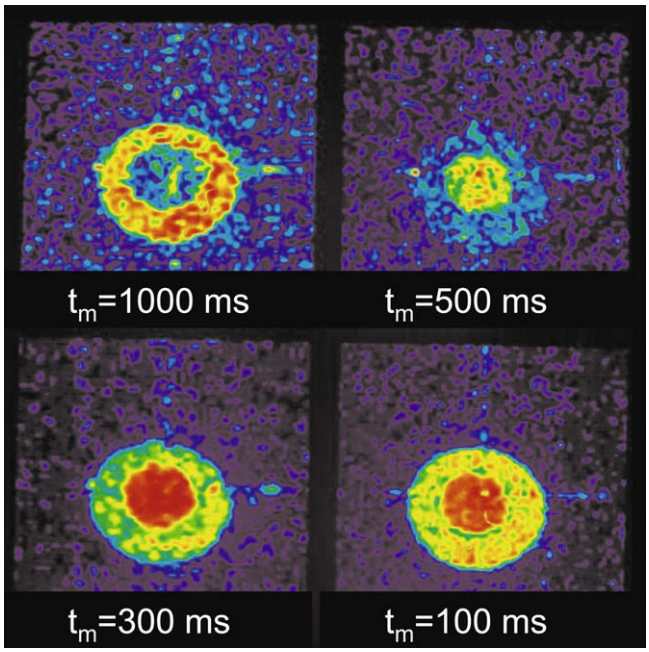

Fig. 12. An example of contrast manipulation by changing encoding times. Reprinted with permission from Planinšič et. al. [9].

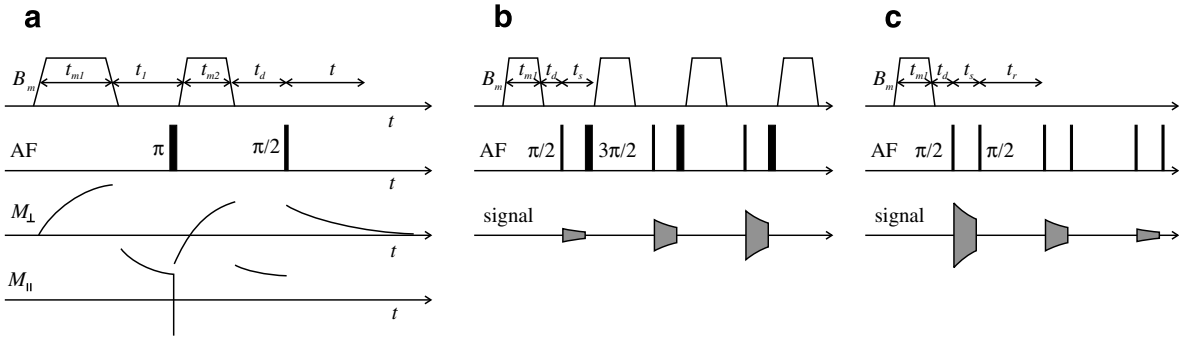

Fig. 11. (a) The magnetization subtraction pulse sequence. (b) The sequence for a single-scan T_1^m measurement. (c) Pulse sequence for a single-scan T_1 measurement.

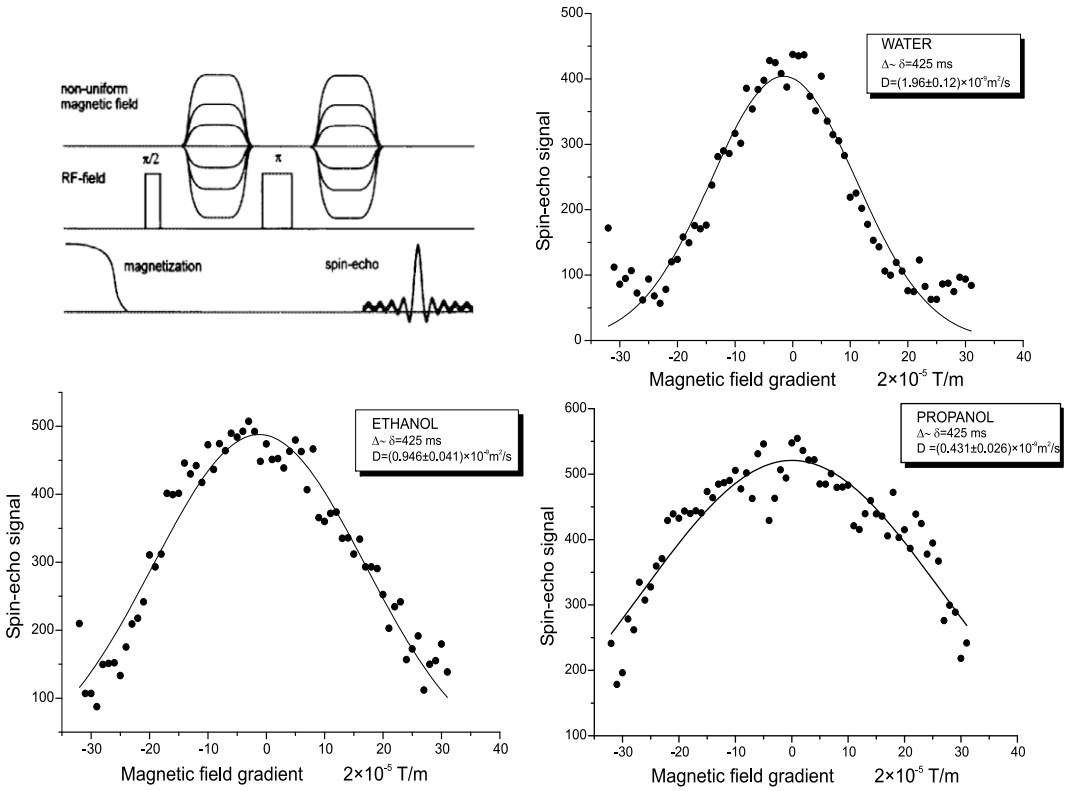

Fig. 13. Spin-echo amplitude as a function of the gradient field for water, ethanol and propanol, and Gaussian fits. Reprinted with permission from Stepišnik et. al. [56].

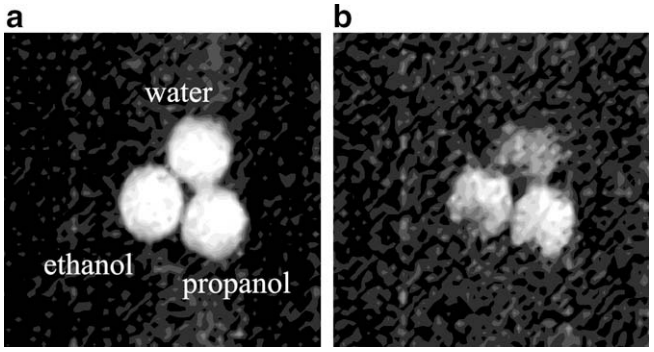

Fig. 14. A 64 × 64 pixel 2D image with 20 cm field of view showing the distribution of the self-diffusion constant as measured by the PGSE and spin warp combination: (a) no diffusion encoding gradient, (b) with gradient (areas with higher self-diffusion constant become darker). The sample under study consisted of three cylindrical tubes each 5 cm in diameter filled with water, ethanol, and propanol. An axial slice thorough the sample is shown. Reprinted with permission from Mohorič et. al. [58].

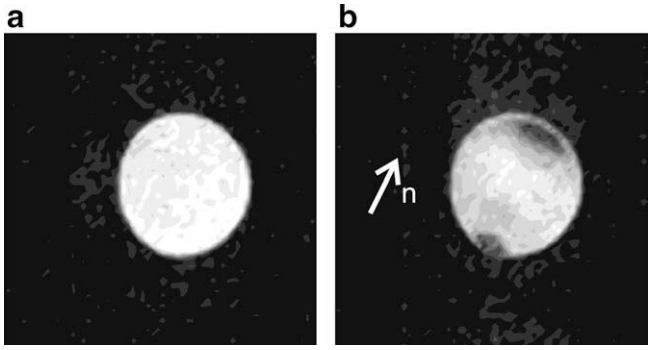

Fig. 15. Diffusion attenuated axial slice of a 10 cm diameter horizontal cylinder filled with propanol: (a) without diffusion encoding gradient pulses, (b) with diffusion encoding – $\Delta \simeq \delta = 200$ ms and $G = 1.8 \times 10^{-3}$ T/m; $\boldsymbol{n}$ denotes the vertical. Larger attenuation (dark spots) appears where the projection of the velocity field along the gradient direction is large. Attenuation is caused by the non-stationary character of free convection. Reprinted with permission from Mohorič and Stepišnik [59].

magnitude G separated by Δ followed by an MRI sequence. Assuming that a molecule j, is displaced by $\delta \boldsymbol{r}_j(t)$ due to random diffusion motion and by $\boldsymbol{v}_j t$ due to convection, then a single shot spin-echo-imaging sequence gives the signal as

$$E(\boldsymbol{k}) \approx E_0 \sum_j \mathrm{e}^{\mathrm{i}\boldsymbol{k}\cdot\boldsymbol{r}_{j0} - \beta_\mathrm{D} + \mathrm{i}\boldsymbol{a}\cdot\boldsymbol{v}_j} \tag{88}$$

where $\boldsymbol{a} = \gamma \boldsymbol{G}\delta(\Delta + \delta)$ and β_D is the diffusion attenuation. Signal averaging with many repetitions of an identical sequence, requires a perfect temperature balance to prevent convection. In our case, a weak temperature gradient and its fluctuations led to the change of $\boldsymbol{v}_j$ between successive sequence applications which gives the averaged signal

$$\overline{E(\boldsymbol{k})} \approx E_0 \sum_j \left(\mathrm{e}^{\mathrm{i}\boldsymbol{k}\cdot\boldsymbol{r}_{j0} - \beta_\mathrm{D}} \times \frac{1}{m} \sum_{s=1}^{m} \mathrm{e}^{\mathrm{i}\boldsymbol{a}\cdot\boldsymbol{v}_{js}} \right) \tag{89}$$

where $\boldsymbol{v}_{js}$ is the convection flow during the application of the sth sequence repetition. With the mean of the convection flow along the applied gradient, $\langle v_j \rangle = \frac{1}{m}\sum_{s=1}^{m} v_{js}$ and its variance, $\langle \delta v_j^2 \rangle = \frac{1}{m}\sum_{s=1}^{m} \langle v_{js} - \langle v_j \rangle \rangle^2$, the averaged spin-echo signal can be approximated as

$$\overline{E(\boldsymbol{k})} \approx E_0 \sum_j \mathrm{e}^{\mathrm{i}\boldsymbol{k}\cdot\boldsymbol{r}_{j0} + \mathrm{i}a\langle v_j \rangle - \beta_\mathrm{D} - \frac{1}{2}a^2 \langle \delta v_j^2 \rangle + \cdots} \tag{90}$$

In addition to the diffusion attenuation β_D, the attenuation proportional to the variance of the convection flow fluctuation appears.

Assuming that the variance is proportional to the mean flow, then the attenuation distribution is the MRI image of the macroscopic convection flow in the container. For a horizontally oriented cylinder where the flow is induced by natural convection, the flow variation (δv) can in the first approximation be calculated from the Lorentz model and exhibits chaotic character [59]. Together with the diffusion encoding inhomogeneous magnetic field (quadrupole field)

$$\boldsymbol{g}_r = \nabla|((Gz + B_0)\cos 30^\circ, (Gz + B_0)\sin 30^\circ, G(x\cos 30^\circ - y \times \sin 30^\circ))| \tag{91}$$

we can calculate the spatial dependence of the attenuation. The magnitude of attenuation is given by the magnitude of the fluctuation rate of the flow.

NMR measurements of velocity fluctuations offer a deeper insight into molecular motion than just a knowledge of the diffusion coefficient. By a proper temporal modulation of the magnetic field gradient, it is possible to measure the diffusion spectrum, as indicated by Eq. (67), if the gradient spectrum has a narrow peak at the modulation frequency akin to the delta function. Gradient modulation can be tailored to a suitable form with a single narrow spectral peak positioned at the measuring frequency. For measurements in the Earth's field we tested a sinusoidally modulated gradient with its amplitude tailored in such a way as to avoid a zero frequency peak in the phase modulation spectrum

$$G(t) = G_0 \sin 2\pi t/T(H[t] + 2H[t - T/2] + H[t - T] - H[t - 3T] - 2H[t - 7T/2] - H[t - 4T])/4 \tag{92}$$

The modulation is represented in Fig. 16.

The spectrum of the phase factor (Fig. 17)

$$|q(\omega)|^2 = \frac{64\pi^2\gamma^2G_0^2T^2\left(\cos\frac{\omega T}{4} + \cos\frac{3\omega T}{4} + \cos\frac{5\omega T}{4}\right)^2 \sin^6\frac{\omega T}{4}}{\omega^2(4\pi^2 - \omega^2T^2)^2} \tag{93}$$

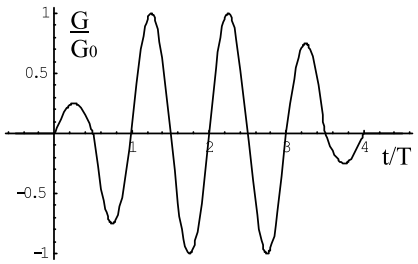

Fig. 16. Gradient modulation for measuring the diffusion spectrum. The amplitude of oscillations is modulated in such way that the zero frequency part of the phase factor spectrum is minimized. To change the frequency at which the spectrum is sampled, the period T is changed. To measure the attenuation, amplitude G_0 is changed.

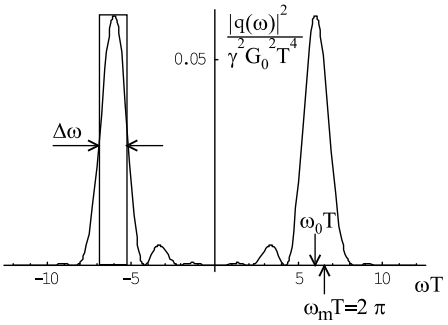

Fig. 17. The spectrum of gradient modulation used for measuring the diffusion spectrum. The sampling frequency (peak of the spectrum) is given by the modulation period $\omega_m = 2\pi/T$, and the spectral resolution $\Delta\omega$ is given by the width of the peak.

has a peak at

$$\omega_0 = \frac{2\pi}{T}\left(1 - \frac{3}{2 + 7\pi^2}\right) = 0.958\ \omega_m \tag{94}$$

($\omega_m = 2\pi/T$) and its spectral resolution is given by

$$\Delta\omega = 0.2987\ \omega_m \tag{95}$$

The attenuation is given by

$$\beta = -\ln E/E_0 = \frac{1}{\pi}\int_0^\infty D(\omega)|q(\omega)|^2\,\mathrm{d}\omega \approx \frac{1}{\pi}D(\omega_0)\int_0^\infty |q(\omega)|^2\,\mathrm{d}\omega = \frac{23}{\pi^2 64}\gamma^2G_0^2T^3D(\omega_0) \tag{96}$$

This sequence was tested by measuring the diffusion spectrum of water. In the Brownian motion approximation, the diffusion spectrum of water is expected to be flat, but the results indicate strong dependence on frequency in the low-frequency part. The results are unexpected and many problems hinder the technique. Refocusing spins into the echo is difficult without π pulses and it is hard to match gradients in modulated sequences. The stability of the field and the transients are another cause for misinterpretation of the results. However, recent measurements of water diffusion spectra $D(\omega)$ in high-magnetic field by a similar method show a similar strong decline at low frequencies. The origin might be in the collective modes of motion of water molecules.

10. Conclusion

Measurements in the Earth's magnetic field offer an inexpensive alternative to strong field NMR. A weak B_0 provides unique experimental conditions comparable only with NMR in the stray field of a superconducting magnet where the effects of strong concomitant gradient components can be studied. In NMR a non-uniform magnetic field can be described by a "magnetic field gradient" only when it is weaker than the main magnetic field, B_0. According to Maxwell's equations, the direction of a magnetic field is changing if the magnetic field is not uniform. This means that there is always more than one component of the field different from zero. Therefore, the magnetic field at a point shifted from the initial position by d$\boldsymbol{r}$ can be written as

$$\boldsymbol{B} = \boldsymbol{B}_0 + \boldsymbol{B}_g(\boldsymbol{r}, t) = \boldsymbol{B}_0 + \mathscr{G}(t)\mathrm{d}\boldsymbol{r} \tag{97}$$

with $\mathscr{G}$ being a tensor. In the case of $B_g \ll B_0$, the magnetic field components perpendicular to the static magnetic field are neglected. The magnetic field gradients are the remaining components of the tensor. This approximation has no meaning whenever the applied non-uniform magnetic field is of the order of or larger than the main magnetic field. However, in a weak main magnetic field the spin-echo response

$$E(t) \approx E_0\sum_j \mathrm{e}^{\mathrm{i}\int_0^t \omega_{\mathrm{eff}}(\boldsymbol{r}_j,t')\mathrm{d}t'} \tag{98}$$

is governed by the effective precession frequency

$$\omega_{\mathrm{eff}}(\boldsymbol{r}_j, t) = \sqrt{(\omega_0 + \gamma B_{gz}(\boldsymbol{r}_j, t))^2 + \gamma^2B_{gy}^2(\boldsymbol{r}_j, t) + \gamma^2B_{gx}^2(\boldsymbol{r}_j, t)} \tag{99}$$

whenever the magnetic field time-variation fulfills the adiabatic condition

$$\frac{\mathrm{d}\omega_{\mathrm{eff}}}{\mathrm{d}t} \ll \omega_{\mathrm{eff}}^2 \tag{100}$$

Thus, to a first approximation, the signal in the vicinity of the spin-echo peak encodes the spin location at $\boldsymbol{r}_j = \boldsymbol{r}_{j0} + \Delta\boldsymbol{r}_j$ as

$$E(t) \approx E_0\sum_j \mathrm{e}^{\mathrm{i}\int_0^t \Delta\boldsymbol{r}_j\cdot\nabla[\omega_{\mathrm{eff}}(\boldsymbol{r}_j,t')]\,\mathrm{d}t'} \tag{101}$$

because $\int_0^\tau \omega_{\mathrm{eff}}(\boldsymbol{r}_{j0},t)\mathrm{d}t \approx 0$; the effective precession frequency changes sign upon application of a π-pulse.

The magnetic field gradient caused by a susceptibility mismatch is much smaller in a weak field which results in a longer signal and helps to increase the S/N. Also the longitudinal and transversal relaxations are different and measurements of relaxation give information on molecular dynamics outside the reach of strong field NMR. Furthermore, field uniformity enables use of large samples and with proper pre-magnetization, shielding and reference detection, S/N can be maintained at reasonably high values.

Appendix A

A.1. Time-evolution

The evolution of the system is governed by the evolution operator $U(t)$ which can be formally expressed by the Hamiltonian $H(t)$

$$U(t) = \widehat{T}\mathrm{e}^{-\mathrm{i}/\hbar\int_0^t H(t')\mathrm{d}t'} = \widehat{T}\mathrm{e}^{-\mathrm{i}/\hbar\int_0^t (H_1(t')+H_2(t'))\mathrm{d}t'} \tag{A.1}$$

A.2. Factorization

If evolution can be written as the product of two operators then

$$U(t) = U_1(t)U_2(t) = \widetilde{U}_2(t)U_1(t) \tag{A.2}$$

with

$$U_1(t) = \widehat{T}\mathrm{e}^{-\mathrm{i}/\hbar\int_0^t H_1(t')\mathrm{d}t'} \tag{A.3}$$

$$U_2(t) = \widehat{T}\mathrm{e}^{-\mathrm{i}/\hbar\int_0^t U_1^{-1}(t')H_2(t')U_1(t')\mathrm{d}t'} \tag{A.4}$$

$$\widetilde{U}_2(t) = \widehat{T}\mathrm{e}^{-\mathrm{i}/\hbar\int_0^t U_1(t')H_2(t')U_1^{-1}(t')\mathrm{d}t'} \tag{A.5}$$

A.3. Perturbation expansion

$$\begin{aligned} U(t) &= \widehat{T}\mathrm{e}^{-\mathrm{i}/\hbar\int_0^t H(t')\mathrm{d}t'} \\ &= 1 + (-\mathrm{i}/\hbar)\int_0^t H(t')\mathrm{d}t' + (-\mathrm{i}/\hbar)^2\int_0^t \mathrm{d}t_1 \\ &\quad\times\int_0^{t_1}\mathrm{d}t_2 H(t_1)H(t_2) + (-i/\hbar)^n\int_0^t \mathrm{d}t_1\int_0^{t_1}\mathrm{d}t_2 \\ &\quad\times\int_0^{t_2}\mathrm{d}t_3 H(t_1)H(t_2)H(t_3) + \cdots \end{aligned} \tag{A.6}$$

A.4. Magnus expansion

A formally written time evolution operator A.1 with a time dependent Hamiltonian requires time ordering by $\widehat{T}$ and one cannot perform integration of the exponent. This can be overcome by coherent averaging. This means that Eq. (A.1) is expanded according to Magnus [90]

$$U(t) = \widehat{T}\mathrm{e}^{-\mathrm{i}/\hbar\int_0^t H(t')\mathrm{d}t'} = \mathrm{e}^{-\mathrm{i}F(t)/\hbar} \tag{A.7}$$

with

$$F(t) = F_0(t) + F_1(t) + F_2(t) + \cdots \tag{A.8}$$

where

$$F_0(t) = \int_0^t H(t')\mathrm{d}t' \tag{A.9}$$

$$F_1(t) = -\frac{i}{2}\int_0^t \mathrm{d}t_1\int_0^{t_1}\mathrm{d}t_2[H(t_1),H(t_2)] \tag{A.10}$$

$$\begin{aligned} F_2(t) = \frac{1}{6}\int_0^t \mathrm{d}t_1\int_0^{t_1}\mathrm{d}t_2\int_0^{t_2}\mathrm{d}t_3\{&[H(t_1),[H(t_2),H(t_3)]] \\ &+[H(t_3),[H(t_2),H(t_1)]]\} \end{aligned} \tag{A.11}$$

Appendix B

B.1. Vector rotation

The rotation of the coordinate system around the unit vector $\boldsymbol{n}$ by an angle φ transforms a vector $\boldsymbol{B}$ into

$$\boldsymbol{B}' = \boldsymbol{B}\cos\varphi + \boldsymbol{n}(\boldsymbol{n}\cdot\boldsymbol{B})(1-\cos\varphi) + (\boldsymbol{n}\times\boldsymbol{B})\sin\varphi \tag{A.12}$$

This expression can be used for the rotation of the vector's sum $\boldsymbol{B} = \boldsymbol{B}_0 + \boldsymbol{B}_1$, with $\boldsymbol{B}_0 = (0,0,b_0)$ and $\boldsymbol{B}_1 = (b_{1x},b_{1y},b_{1z})$ to be aligned along the z-axis

$$\boldsymbol{n} = \frac{\boldsymbol{B}_1\times\boldsymbol{B}_0}{|\boldsymbol{B}_1\times\boldsymbol{B}_0|} = \frac{(b_{1y},-b_{1x},0)}{\sqrt{b_{1x}^2+b_{1y}^2}} \tag{A.13}$$

$$\sin\varphi = \frac{|(\boldsymbol{B}_0+\boldsymbol{B}_1)\times\boldsymbol{B}_0|}{|\boldsymbol{B}_0+\boldsymbol{B}_1|.|\boldsymbol{B}_0|} = \sqrt{\frac{b_{1x}^2+b_{1y}^2}{b_{1x}^2+b_{1y}^2+(b_{1z}+b_0)^2}} \tag{A.14}$$

$$\cos\varphi = \frac{(\boldsymbol{B}_0+\boldsymbol{B}_1)\cdot\boldsymbol{B}_0}{|\boldsymbol{B}_0+\boldsymbol{B}_1||\boldsymbol{B}_0|} = \frac{b_{1z}+b_0}{\sqrt{b_{1x}^2+b_{1y}^2+(b_{1z}+b_0)^2}} \tag{A.15}$$

The rotation vector that transforms $\boldsymbol{B}$ into

$$\boldsymbol{B}' = \left(0,0,\sqrt{b_{1x}^2+b_{1y}^2+(b_{1z}+b_0)^2}\right) \tag{A.16}$$

is defined as

$$\boldsymbol{\varphi} = \boldsymbol{n}\varphi = \frac{(b_{1y},-b_{1x},0)}{\sqrt{b_{1x}^2+b_{1y}^2}}\arctan\frac{\sqrt{b_{1x}^2+b_{1y}^2}}{b_{1z}+b_0}$$

B.2. Reversed helmholtz coil

A reversed Helmholtz coil together with a uniform magnetic field pointing parallel to the coil axis creates a non-uniform magnetic field $\boldsymbol{B} = (Gx,Gy,2G(z-z_0)+B_0)$ in a wide region inside the coil. The gradient of the field magnitude is

$$\nabla|\boldsymbol{B}| = G\frac{(Gx,Gy,2[2G(z-z_0)+B_0])}{\sqrt{(Gx)^2+(Gy)^2+[2G(z-z_0)+B_0]^2}} \tag{A.17}$$

$$= \boldsymbol{f}(x,y,z,t) \tag{A.18}$$

The spin-echo signal appears from Eqs. (48) and (58) as

$$E(\tau) = E_0\sum_j \mathrm{e}^{-\gamma^2 D\int_0^\tau\int_0^t \boldsymbol{f}(x,y,z,t_1)\mathrm{d}t_1\int_0^t \boldsymbol{f}(x,y,z,t_2)\mathrm{d}t_2\,\mathrm{d}t}. \tag{A.19}$$

The attenuation depends upon the spin location in the sample and the extraction of the self-diffusion constant from Eq. (A.19) might be a very complex problem.

Only in the case $B_g \ll B_0$ can Eq. (A.18) be approximated as

$$(\nabla|\boldsymbol{B}|)^2 = 4G^2 \tag{A.20}$$

and we can use the usual expression for the spin-echo attenuation.

Appendix C

C.1. Gaussian approximation

According to the theory of stochastic processes [91], Eq. (51) has the form of a characteristic functional of a stochastic process with $\boldsymbol{v}_j(t)$ as a stochastic variable and $\boldsymbol{q}_j(t)$ as a test function. A characteristic functional describes the stochastic process as well as the probability distribution and can be expressed by the autocorrelation functions of the stochastic variables using the cumulant expansion as

$$\left\langle e^{i\int_0^\tau \boldsymbol{q}_j(t)\cdot\boldsymbol{v}_j(t)dt}\right\rangle = e^{J_j(\tau)} \tag{A.21}$$

where the cumulant function is the infinite series

$$J(\tau) = i\int_0^\tau \boldsymbol{q}(t_1)\cdot\langle\boldsymbol{v}(t_1)\rangle dt' - \frac{1}{2}\int_0^\tau\int_0^\tau \langle \boldsymbol{q}(t_1)\cdot\boldsymbol{v}(t_1)\boldsymbol{q}(t_2)\cdot\boldsymbol{v}(t_2)\rangle_c dt_1 dt_2 - i\frac{1}{6}\int_0^\tau\int_0^\tau\int_0^\tau \langle \boldsymbol{q}(t_1)\cdot\boldsymbol{v}(t_1)\boldsymbol{q}(t_2)\cdot\boldsymbol{v}(t_2)\boldsymbol{q}(t_3)\cdot\boldsymbol{v}(t_3)\rangle_c dt_1 dt_2 dt_3 + \cdots \tag{A.22}$$

For simple Brownian motion, the velocity auto-correlation function decays rapidly to zero over the correlation time τ_c, corresponding to the average molecular collision time. The value of τ_c is exceedingly short for the time regime accessible to the spin echo sequence, which is longer than 10^{-5} s. The cumulant terms almost vanish unless the time points in them differ by less than an order of τ_c, and the entire contribution to the m-fold integral of the series Eq. (A.22) arises from the domain of order $t\tau_c^{m-1}$. One can estimate the convergence of the cumulant series by denoting the magnitude of velocity fluctuation as (∂v) which is related to the diffusion coefficient as

$$D = \frac{1}{3}\int_0^\infty \langle \boldsymbol{v}(t)\boldsymbol{v}(0)\rangle_c dt \approx (\partial v)^2\tau_c, \tag{A.23}$$

Approximating $q(t)\approx F$, Eq. (A.22) is an expansion in powers of $q(\partial v)\tau_c$, with each term being roughly linear in time. The mth term of the cumulant series is of the order of

$$q^2(\partial v)^2\tau_c[q(\partial v)\tau_c]^{m-2}t. \tag{A.24}$$

In the limit of

$$q(\partial v)\tau_c \ll 1, \quad \text{and} \quad q^2(\partial v)^2\tau_c t = \text{finite} \tag{A.25}$$

all cumulants higher than the second can be omitted. The Gaussian phase approximation is valid as long as the gradient is weak enough, so that $q(\partial v)\tau_c \approx ql \ll 1$ where l denotes a molecular mean free path and $1/q$ as the length of the spin phase grating created by the applied gradient.

For gases at room temperature and atmospheric pressure, the mean free path is about 100 nm giving for a 1 ms long gradient pulse a limiting amplitude of the gradient of about 40 T/m. However, in liquids it is higher by about two orders of magnitude, which is above the practical attainability of gradients of conventional coils.

However, in the case of macromolecular and restricted molecular motion in porous media some characteristic times can be much longer. The use of the Gaussian phase approximation requires caution, for instance, when the gradient phase grating is larger than the size of the compartments in the porous media.

References

[1] M. Packard, R. Varian, Free nuclear induction in the Earth's magnetic field, Phys. Rev. 93 (1954) 941.
[2] G.J. Bene, Nuclear magnetism of liquid systems in the Earth field range, Phys. Rep. 58 (1980) 213–267.
[3] A.G. Anderson, Nonresonant nuclear spin absorption in lithium, sodium, and aluminum, Phys. Rev. 115 (1959) 863–868.
[4] A.G. Anderson, Nuclear spin absorption spectra in solids, Phys. Rev. 125 (1962) 1517–1527.
[5] A. Abragam, The Principles of Nuclear Magnetism, Clarendon, Oxford, 1961.
[6] M.P. Borodin, A.V. Mel'nikov, A.A. Morozov, Y.S. Chernyshev, Nuclear Magnetic Resonance in the Earth Field, Leningrad State University, 1967 (in Russian).
[7] S.H. Koenig, D. Adams, D. Emerson, C.G. Harrison, Research report RC 10116, IBM Research division, 1983.
[8] G.J. Bene, B. Borgard, E. Hiltbrand, P. Magnin, *In situ* identification of human physiological fluids by nuclear magnetism in the Earth's field, Phil. Trans. R. Soc. Lond. B 289 (1980) 501–502.
[9] G. Planinšič, J. Stepišnik, M. Kos, Relaxation-time measurement and imaging in the Earth's magnetic-field, J. Magn. Reson. A 110 (1994) 170–174.
[10] D. Kleppner, MRI for the third world, Phys. Today (1992) 9–10.
[11] J. Stepišnik, Feasibility of NMR Imaging in Earth field range, Proceedings of XXII Congress Ampere (1984) 528–529.
[12] J. Stepišnik, D. Mihajlovič, NMR Imaging by Earth's Magnetic Field, Abstracts of 7th specialized colloque Ampere, Bucharest, 1985, p. 194.
[13] H. Mehier, M. Maurice, J.P. Bonche, G. Jacquemod, C. Desuzinges, B. Favre, J.O. Peyrin, Imagierie par resonance magnetique nucleaire en champ tres faible, J. Biophys. Biomed. 9 (1985) 198.
[14] J. Stepišnik, M. Kos, V. Eržen, in: B. Maraviglia et al. (Eds.), Selective magnetization at magnetic resonance imaging in low field, Proceedings of XXII Congress AMPERE on Magnetic Resonance, Instituto Superiore di Sanita, Romas, 1986, p. 512.
[15] J. Stepišnik, V. Eržen, D. Mihailovic, NMR imaging by Earth's magnetic field, in: Proceedings of 8th European Experimental NMR Conference, 1986, p. 145.
[16] J. Stepišnik, V. Eržen, D. Mihailovic, B.B. Lavrenčič, A. Čadež, NMR imaging in Earth's magnetic field, Farm. Vest. 37 (1986) 135–137.
[17] P. Mansfield, P.G. Morris, NMR Imaging in Biomedicine, Academic Press, 1982.
[18] P.T. Callaghan, M. Legros, Nuclear spins in the Earth's magnetic field, Am. J. Phys. 50 (1982) 709–713.
[19] A. Mohorič, G. Planinšič, M. Kos, A. Duh, J. Stepišnik, Magnetic resonance imaging based on Earth's magnetic field, Instrum. Sci. Technol. 32 (2004) 655–667.
[20] M.E. Halse, A. Coy, R. Dykstra, C. Eccles, M. Hunter, R. Ward, P.T. Callaghan, A practical and flexible implementation of 3D MRI in the Earth's magnetic field, J. Magn. Reson. 182 (2006) 75–83.
[21] J. Stepišnik, V. Eržen, M. Kos, NMR imaging in the Earth's magnetic field, Magn. Reson. Med. 15 (1990) 386–391.
[22] P.T. Callaghan, C.D. Eccles, NMR studies on Antarctic Sea Ice, Bull. Magn. Reson. 18 (1996) 62–64.
[23] P.T. Callaghan, C.D. Eccles, T.G. Haskell, P.J. Langhorne, J.D. Seymour, Earth's field NMR in Antarctica: a pulsed gradient spin echo NMR study of restricted diffusion in Sea Ice, J. Magn. Reson. 133 (1998) 148–154.
[24] P.T. Callaghan, C.D. Eccles, J.D. Seymour, An Earth's field nuclear magnetic resonance apparatus suitable for pulsed gradient spin echo measurements of self-diffusion under Antarctic conditions, Rev. Sci. Instrum. 68 (1997) 4263–4270.
[25] P.T. Callaghan, R. Deykstra, C.D. Eccles, T.G. Haskell, J.D. Seymour, A nuclear magnetic resonance study of Antarctic sea ice brine diffusivity, Cold Reg. Sci. Technol. 29 (1999) 153–171.
[26] O.R. Mercier, M.W. Hunter, P.T. Callaghan, Brine diffusion in first-year sea ice measured by Earth's field PGSE-NMR, Cold Reg. Sci. Technol. 42 (2005) 96–105.
[27] A. Shushakov, Groundwater NMR in conductive water, Geophysics 61 (1996) 998–1006.
[28] D.V. Trushkin, O.A. Shushakov, A.V. Legchenko, The potential of a noise-reducing antenna for surface NMR groundwater surveys in the Earth's magnetic field, Geophys. Pros. 42 (1994) 855–862.
[29] E. Duval, J. Ranft, G. Bene, Determination des signes relatifs des constantes de couplage 31 p- 1 h dans le tripropyl phosphate par r.m.n. dans le champ magnetique terrestre, Mol. Phys. 9 (1965) 427–431.
[30] C.A. Meriles, D. Sakellariou, D.H. Heise, A.J. Moule, A. Pines, Approach to high-resolution ex situ NMR spectroscopy, Science 293 (2001) 82–85.
[31] J. Perlo, V. Demas, F. Casanova, C.A. Meriles, J. Reimer, A. Pines, B. Blumich, High-resolution NMR spectroscopy with a portable single-sided sensor, Science 308 (2005) 1279.
[32] S. Appelt, F.W. Hasing, H. Kuhn, J. Perlo, B. Blumich, Mobile high resolution xenon nuclear magnetic resonance spectroscopy in the Earth's magnetic field, Phys. Rev. Lett. 94 (2005) 197–602.
[33] S. Appelt, H. Kuhn, F.W. Hasing, B. Blumich, Chemical Analysis by ultrahigh-resolution nuclear magnetic resonance in the Earth's magnetic field, Nat. Phys. 2 (2006) 105–109.
[34] J.N. Robinson, A. Coy, R. Dykstra, C.D. Eccles, M.W. Hunter, P.T. Callaghan, Two-dimensional NMR spectroscopy in Earth's magnetic field, J. Magn. Reson. 182 (2006) 343–347.
[35] M. Burghoff, S. Hartwig, L. Trahms, J. Bernarding, Nuclear magnetic resonance in the nanoTesla range, Appl. Phys. Lett. 87 (2005) 54–103.
[36] R. McDermott, A.H. Trabesinger, M. Muck, E.L. Hahn, A. Pines, J. Clarke, Liquid-state NMR and scalar couplings in microtesla magnetic fields, Science 295 (2002) 2247–2249.
[37] S. Appelt, F.W. Hasing, H. Kuhn, U. Sieling, B. Blumich, Analysis of molecular structures by homo- and hetero-nuclear *J*-coupled NMR in ultra-low field, Chem. Phys. Lett. 440 (Issues 4-6) (2007) 308–312.
[38] D.B. Zax, A. Bielecki, K.W. Zilm, A. Pines, D.P. Weitencamp, Zero field NMR and NQR, Chem. Phys. 83 (1985) 4877–4905.
[39] M. Kohl, M. Odehnal, V. Petricek, R. Tichy, S. Safrata, Observation of higher order NMR Larmor lines by SQUID in solids at low magnetic field, J. Low Temp. Phys. 72 (1988) 319–343.
[40] C.P. Slichter, Principles of Magnetic Resonance, Springer-Verlag, Berlin, 1990.
[41] A. Abragam, M. Goldman, Nuclear Magnetism: Order and Disorder, Clarendon, Oxford, 1982.
[42] E. Hiltbrand, B. Borcard, R. Sechehaye, G. Bene, Frequency shifts in nuclear spin system, Helv. Phys. Acta 49 (1976) 163–167.
[43] W. Happer, Optical pumping, Rev. Mod. Phys. 44 (1972) 169–249.

[44] J. Clarke, in: H. Weinstock (Ed.), SQUID Sensors: Fundamentals, Fabrication and Applications, Kluwer Academic, Dordrecht, The Netherlands, 1996, pp. 1–62.
[45] Y.S. Greenberg, Application of superconducting quantum interference devices to nuclear magnetic resonance, Rev. Mod. Phys. 70 (1998) 175–222.
[46] H.C. Seton, J.M.S. Hutchison, D.M. Bussell, A 4.2 K receiver coil and SQUID amplifier used to improve the SNR of low field magnetic resonance images of the human arm, Meas. Sci. Technol. 8 (1997) 198–207.
[47] S. Kumar, B.D. Thorson, W.F. Avrin, Broadband SQUID NMR with room-temperature samples, J. Magn. Reson. B 107 (1995) 252–259.
[48] K. Schlenga, R. McDermott, J. Clarke, R.E. de Souza, A. Wong-Foy, A. Pines, Low-Field magnetic resonance imaging with a high-Tc DC SQUID, Appl. Phys. Lett. 75 (1999) 3695–3697.
[49] A.H. Trabesinger, R. McDermott, S. Lee, M. Mück, J. Clarke, A. Pines, Squid-detected liquid state nmr in microtesla fields, IEEE Trans. Appl. Superconduc. 108 (2004) 2936–2957.
[50] P.T. Callaghan, M. Halse, A. Coy, R. Dykstra, C. Eccles, M. Hunter, R. Ward, A practical and flexible implementation of 3D MRI in the Earth's magnetic field, J. Mag. Res. 182 (2006) 75–83.
[51] V.S. Zotev, A.N. Matlachov, P.L. Volegov, H.J. Sandin, M.A. Espy, J.C. Mosher, A.V. Urbaitis, S.G. Newman, R.H. Kraus Jr., Multi-channel SQUID system for meg and ultra-low-field MRI, IEEE T. Appl. Supercon. 17 (2) (2007) 839–842.
[52] B.F. Melton, V.L. Pollak, Instrumentation for the Earth's field NMR technique, Rev. Sci. Instrum. 42 (1971) 769–773.
[53] B. Favre, J.P. Bonche, H. Mehier, J.O. Peyrin, Environmental optimization and shielding for NMR experiments and imaging in the Earth's magnetic field, Magn. Reson. Med. 13 (1990) 299–304.
[54] R.L. Kleinberg, in: B.M. Grant, R.K. Harro (Eds.), Encyclopedia of Magnetic Resonance, Wiley, New York, 1995, p. 4960.
[55] B.F. Melton, V.L. Pollak, T.W. Mayes, B.L. Willis, Condition for sudden passage in the Earth's-Field NMR technique, J. Magn. Reson. A 117 (1996) 164–170.
[56] J. Stepišnik, M. Kos, G. Planinšič, V. Eržen, Strong non-uniform magnetic field for a self-diffusion measurement by NMR in the Earth's magnetic field, J. Magn. Res. A 107 (1994) 167–172.
[57] M. Kos, Magnetic resonance in a weak magnetic field for self-diffusion measurement and flow, Ph.D. Thesis, University of Ljubljana, 1992.
[58] A. Mohorič, J. Stepišnik, M. Kos, G. Planinšič, Self-diffusion imaging by spin echo in Earth's magnetic field, J. Magn. Reson. 136 (1999) 22–26.
[59] A. Mohorič, J. Stepišnik, The effect of natural convection in horizontally oriented cylinder on NMR imaging of the distribution of diffusivity, Phys. Rev. E 62 (2000) 6615–6627.
[60] S. Chapman, The Earth's Magnetism, Methuen, London, 1951.
[61] T. Jochimsen, A. Schafer, R. Bammer, M. Moseley, Efficient simulation of magnetic resonance imaging with Bloch-Torrey equations using intra-voxel magnetization gradients, J. Mag. Res. 180 (2006) 29–38.
[62] D.J. Sloop, T.S. Lin, J.J.H. Ackerman, Transient magnetic resonance without RF pulses: fast field switching, J. Mag. Res. 139 (1999) 60–66.
[63] R.M. Wilcox, Exponential operators and parameter differentiation in quantum physics, J. Math. Phys. 8 (1967) 962–982.
[64] W.A.B. Evans, On some application of the Magnus expansion in nuclear magnetic resonance, Ann. Phys. 48 (1968) 72–93.
[65] J. Stepišnik, NMR measurement and Brownian movement in the short-time limit, Phys. B 198 (1994) 299–306.
[66] J. Stepišnik, Violation of the gradient approximation in NMR self-diffusion measurements, Z. Phys. Chem. 190 (1995) 51–62.
[67] N. Blombergen, E.M. Purcell, R.V. Pound, Relaxation effects in nuclear magnetic resonance absorption, Phys. Rev. 73 (1948) 679–712.
[68] E.L. Hahn, Spin-echoes, Phys. Rev. 80 (1950) 580–594.
[69] H.Y. Carr, E.M. Purcell, Effects of diffusion on free precession in nuclear magnetic resonance, Phys. Rev. 94 (1954) 630–638.
[70] E.O. Stejskal, Use of spin echoes in a pulsed magnetic-field gradient to study anisotropic, restricted diffusion and flow, J. Chem. Phys. 43 (1965) 3597.
[71] E.O. Stejskal, J.E. Tanner, Spin Diffusion measurements: spin echoes in the presence of a time-dependent field gradient, J. Chem. Phys. 42 (1965) 288.
[72] H.C. Torrey, Bloch equations with diffusion terms, Phys. Rev. 104 (1956) 563–565.
[73] R. Barbe, M. Leduc, F. Laloë, Résonance magnétique en champ de radiofréquence inhomogéne, J. Phys. 35 (1974) 935–951.
[74] J. Stepišnik, Magnetic resonance with nonuniform radiofrequency field, J. Phys. 39 (1978) 689–692.
[75] D. Canet, B. Diter, A. Belmajdoub, J. Brondeau, J.C. Boubel, K. Elbayed, Self-diffusion measurements using a radiofrequency field gradient, J. Magn. Res. 81 (1989) 1–12.
[76] J. Kärger, W. Heink, The propagator representation of molecular transport in microporous crystallites, J. Magn. Reson. 51 (1983) 1–7.
[77] P.T. Callaghan, Principles of Nuclear Magnetic Resonance Microscopy, University Press (Oxford), Oxford, 1991.
[78] J. Stepišnik, Validity limits of gaussian approximation in cumulant expansion for diffusion attenuation of spin echo, Physica B 270 (1999) 110–117.
[79] J. Stepišnik, A new view of the spin echo diffusive diffraction in porous structures, Europhys. Lett. 60 (2002) 453–459.
[80] D.F. Hoult, P.C. Lauterbur, The sensitivity of the zeugmatographic experiment involving human samples, J. Magn. Res. 34 (1979) 425–433.
[81] G. Oedberg, L. Oedberg, On the use of a quadrupole coil for NMR spin-echo diffusion studies, J. Magn. Reson. 16 (1974) 342–347.
[82] G. Planinšič, MRI of relaxation times by magnetic resonance in a weak magnetic field, Ph.D. Thesis, University of Ljubljana, 1993.
[83] G. Planinšič, Shielding of low-frequency magnetic interference in weak-field MRI by a single-layer cylindrical coil, J. Magn. Reson. 126 (1997) 30–38.
[84] A. Duh, Restricted diffusion and edge enhancement at NMR microscopy, B.Sc. Thesis, University of Ljubljana, 1994.
[85] E.A. Edelstein, J.M.S. Hutchinson, G. Johnson, T. Redpath, Spin warp NMR imaging and applications to human whole-body imaging, Phys. Med. Biol. 25 (1980) 751–798.
[86] O. Nalcioglu, Phys. Med. 6 (1990) 175.
[87] A. Caprihan, E. Fukushima, Flow measurements by NMR, Phys. Rep. 198 (1990) 195–235.
[88] T.L. James, A.R. Margulis (Eds.), Biomedical Magnetic Resonance, Radiology Research and Education Foundation, San Francisco, 1984.
[89] J. Stepišnik, Measuring and imaging of flow by NMR, Prog. NMR Spectrosc. 17 (1985) 187–209.
[90] W. Magnus, On the exponential solution of differential equations for a linear operator, Pure Appl. Math. 7 (1954) 649–673.
[91] N. van Kampen, Stochastic Processes in Physics and Chemistry, North-Holland Publishing Company, Amsterdam, 1981.